JOURNAL OF GEOPHYSICAL RESEARCH, VOL. 100, NO. B7, PAGES 12,959–12,983, JULY 10, 1995

Slip patterns and earthquake populations along different classes of faults in elastic solids

Yehuda Ben-Zion and James R. Rice

Department of Earth and Planetary Sciences and Division of Applied Sciences, Harvard University, Cambridge, Massachusetts

Abstract. Numerical simulations of slip instabilities on a vertical strike-slip fault in an elastic half-space are performed for various models belonging to two different categories. The first category consists of inherently discrete cellular fault models. Such are used to represent fault systems made of segments (modeled by numerical cells) that can fail independently of one another. Their quasi-independence is assumed to provide an approximate representation of strong fault heterogeneity, due to geometric or material property disorder, that can arrest ruptures at segment boundaries. The second category consists of models having a well-defined continuum limit. These involve a fault governed by rate- and state-dependent friction and are used to evaluate what types of property heterogeneity could lead to the quasi-independent behavior of neighboring fault segments assumed in the first category. The cases examined include models of a cellular fault subjected to various complex spatial distributions of static to kinetic strength drops, and models incorporating rate- and state-dependent friction subjected to various spatial distributions of effective stress (normal stress minus pore pressure). The results indicate that gradual effective stress variations do not provide a sufficient mechanism for the generation of observed seismic response. Strong and abrupt fault heterogeneity, as envisioned in the inherently discrete category, is required for the generation of complex slip patterns and a wide spectrum of event sizes. Strong fault heterogeneity also facilitates the generation of rough rupture fronts capable of radiating high-frequency seismic waves. The large earthquakes in both categories of models occur on a quasi-periodic basis; the degree of periodicity increases with event size and decreases with model complexity. However, in all discrete segmented cases the models generate nonrepeating sequences of earthquakes, and the nature of the large (quasi-periodic) events is highly variable. The results indicate that expectations for regular sequences of earthquakes and/or simple repetitive precursory slip patterns are unrealistic. The frequency-size (FS) statistics of the small failure episodes simulated by the cellular fault models are approximately self-similar with $b \approx 1.2$ and $b_A \approx 1$, where b and b_A are b values based on magnitude and rupture area, respectively. For failure episodes larger than a critical size, however, the simulated statistics are strongly enhanced with respect to self-similar distributions defined by the small events. This is due to the fact that the stress concentrated at the edge of a rupture expanding in an elastic solid grows with the rupture size. When the fault properties (e.g., geometric irregularities) are characterized by a narrow range of size scales, the scaling of stress concentrations with the size of the failure zone creates a critical rupture area terminating the self-similar earthquake statistics. In such systems, events reaching the critical size become (on the average) unstoppable, and they continue to grow to a size limited by a characteristic model dimension. When, however, the system is characterized by a broad spectrum of size scales, the above phenomena are suppressed and the range of (apparent) self-similar FS statistics is broad and characterized by average b and b_A values of about 1. The simulations indicate that power law extrapolations of low-magnitude seismicity will often underestimate the rate of occurrence of moderate and large earthquakes. The models establish connections between features of FS statistics of earthquakes (range of self-similar regimes, local maxima) and structural properties of faults (dominant size scales of heterogeneities, dimensions of coherent brittle zones). The results suggest that observed FS statistics can be used to obtain information on crustal thickness and fault zone structure.

Introduction

Fault zone properties governing seismic response include, among other things, the distributions of geometrical irregularities (e.g., kinks, jogs, and subparallel strands), material heterogeneities, temperature, and effective stress (normal stress minus pore pressure). Since the above distributions are complex functions of space (and time), the distributions of fault friction and earthquake stress drops can be rather involved.

One class of models for the evolution of stress and slip on faults employs constitutive stress-slip relations based on laboratory sliding experiments. These include models using slip-weakening constitutive law [e.g., *Stuart and Mavko*, 1979; *Day*, 1982; *Andrews*, 1985; *Stuart et al.*, 1985; *Stuart*,

Copyright 1995 by the American Geophysical Union

Paper number 94JB03037
0148-0227/95/94JB-03037$05.00

1986] and rate- and state-dependent friction [e.g., *Dieterich*, 1986, 1992; *Tse and Rice*, 1986; *Okubo*, 1989; *Horowitz and Ruina*, 1989; *Rice*, 1993]. These models are attractive since they incorporate experimentally derived descriptions of the frictional process that can be used to simulate stable sliding, catastrophic failure and, most importantly, the transition between these two modes of slip. However, it is not yet clear whether and how laboratory friction results, based on small rock samples with relatively smooth slip surfaces, correspond to properties of a natural fault system having a wide range of geometrical heterogeneities, as well as far larger slips (and slip rates) during instabilities and longer interseismic intervals for fault rehealing.

Another modeling approach, employing theoretical solutions from fracture mechanics, prescribes fault properties in terms of critical energy release rate, or critical stress intensity factor, characterizing cohesive material forces that resist sliding [e.g., *Kostrov*, 1966; *Virieux and Madariaga*, 1982; *Gao et al.*, 1991; *Yamashita and Knopoff*, 1992; *Yamashita*, 1993; *Rice et al.*, 1994]. As discussed by *Rice* [1980], the description of fault properties in terms of critical energy release rate (or critical stress intensity factor) corresponds to a description based on laboratory-derived constitutive laws in the limiting case when (1) the "critical slip distance," characterizing the evolution of frictional properties with slip, is sufficiently small that the zone of strength degradation is small compared to other model dimensions, and (2) the shear stress on the fault is relatively independent of slip rate or history for slips greater than the critical distance.

A third modeling approach, not addressing the physics of the transition in the frictional properties of sliding surfaces, simply prescribes various distributions of static/kinetic frictions or earthquake stress drops on a fault. This approach, formally corresponding to a case of zero critical slip distance and additional simplifications neglecting the dependence of fault strength on slip velocity, was used in the past [e.g., *Andrews*, 1980, 1981; *Kagan and Knopoff*, 1981; *Kagan*, 1982; *Mikumo and Miyatake*, 1983; *Rundle*, 1988; *Frankel*, 1991; *Ben-Zion and Rice*, 1993] and is adopted in much of the present work, in attempts to elucidate general characteristics of fault response to various complex distributions of properties. *Ben-Zion and Rice* [1993] argued that this third approach could provide a valid approximate treatment of strong geometrical or material property variations which can stop ruptures. Using cells of a numerical grid as an approximate representation of fault segments, delimited by such potentially arresting heterogeneities, the approach may be justified when the nucleation size of slip instabilities (e.g., h^* of *Rice* [1993]) is much smaller than fault segment size.

A key conceptual issue is whether the spatio-temporal complexity of fault slip can be attributed purely to fault dynamics or whether nonuniformities in geometry, material properties, effective stress, and/or mode of loading are essential for understanding the observed complex fault slip. That is, are seismicity in the crust and turbulent flow in a fluid of uniform physical properties analogous as advocated by, e.g., *Kagan* [1994]? A number of recent theoretical studies indicate that the answer may be positive. *Horowitz and Ruina* [1989] generated complex spatial and temporal slip events in a homogeneous model using a rate- and state-dependent friction law, although their model was chosen to weaken long range interactions, so that stress concentrations ahead of sufficiently long ruptures do not increase with length, and they selected a model viscosity parameter to limit stress drop and slip rate ranges during "instabilities." *Bak and Tang* [1989], *Ito and Matsuzaki* [1990], *Lomnitz-Adler* [1993], and others modeled earthquake dynamics using cellular automata governed by simple system evolution rules. *Carlson and Langer* [1989], *Carlson et al.* [1991], and others modeled fault dynamics with extended arrays of *Burridge and Knopoff* [1967] spring-connected blocks and pure velocity dependence of friction. However, these models are problematic since (1) they have system dimension the same as that of the fault, rather than one greater, (2) they employ simplified stress transfer laws (i.e., nearest-neighbor interactions) that do not scale with rupture size in a way suitable to represent faults embedded in elastic continua, and (3) they contain strong implicit heterogeneities in the form of inherent model discreteness and/or highly heterogeneous initial and/or boundary conditions (see below).

Rice [1993] and *Ben-Zion and Rice* [1993] studied mechanical instabilities along two-dimensional (2-D) fault zones embedded in three-dimensional (3-D) elastic solids. The work of Rice involved a smooth fault surface governed by rate- and state-dependent friction, while the work of Ben-Zion and Rice focused on cellular fault structure governed by static/kinetic friction. The procedures account approximately for inertial features by incorporating dynamic overshoot or a radiation damping term. *Rice* [1993] found that there are fundamental differences between models of fault instabilities using separate classes of constitutive laws. When the constitutive stress-slip relation includes a finite critical slip distance over which the strength of failing elements evolves continuously, i.e., a slip weakening or state transition slip distance, the model has a well-defined continuum limit which can be approached for small enough numerical cells. When, however, the strength of failing elements drops discontinuously with slip (as in the cellular automata models mentioned above and the work of Ben-Zion and Rice) or is dependent only on the velocity of slip such that no finite distance is included in the constitutive law (as in the cited block-spring simulations), the model is inherently discrete. In models with a continuum limit, suitably refined cells can fail only as members of a cooperating group, whereas in inherently discrete models, cells can fail individually regardless of how small they are. When a continuum limit exists, the cell size h of a suitably refined grid must be small compared to a nucleation size of slip instabilities h^* (see the analysis section for definition of and additional discussion on h^*). The results of *Rice* [1993] suggest that the generic response of models with a continuum limit, using suitably refined cells and gradual variations of material properties, is a simple limit cycle of repeated earthquakes without a Gutenberg-Richter (GR) spectrum of small events. In contrast, the generic response of inherently discrete systems gives a spectrum of event sizes with some range of self-similar scaling. We note that the work done so far does not rule out the possibility that proper elastodynamic solutions of smooth uniform fault models with a continuum limit would lead to residual stress heterogeneity that can sustain complex seismic response. Recent advocates of this hypothesis [e.g., *Cochard and Madariaga*, 1994; *Shaw*, 1994; *Madariaga and Cochard*, 1994] have attempted to overcome the model discreteness problem. However, the Cochard and Madariaga results are still based on models with strong implicit heterogeneities in the

form of highly heterogeneous initial and boundary conditions (e.g., infinitely strong, wave reflecting, barriers at model edges), and the Shaw modeling involves truncation of stress concentration by approximate elastic coupling to a foundation in a way justifiable only for ruptures much longer than the seismogenic depth. Recently, Y. Ben-Zion, J. R. Rice and G. Zheng (manuscript in preparation, 1995) developed a model incorporating precise elastodynamic treatment of instability episodes into the crustal-scale framework with depth-variable, laboratory-constrained, rate- and state-dependent friction of *Rice* [1993] and the second analysis section of the present paper. In contrast to other works on the subject, this model has natural boundary, (evolving) initial, loading, and arrest conditions, and it provides a proper framework for simulations over many earthquake cycles that may give definitive results on the capacity of inertial dynamics to generate complexity on a smooth fault. Preliminary 2-D simulations (slip variable with depth only) with the model of Y. Ben-Zion et al. do not support the conclusion that dynamics alone could provide a sufficient generic mechanism for sustained generation of complexities [J. R. Rice and Y. Ben-Zion, Slip complexity in earthquake fault models, submitted to *Proc. Natl. Acad. Sci. U. S. A.*, 1995; hereinafter referred to as Rice and Ben-Zion, submitted manuscript, 1995]. We also note that 2-D in-plane calculations of *Andrews* [1975] for dynamic ruptures along a uniform surface characterized by a gradual transition between static and kinetic frictions give, in all calculated cases, final stress distributions that are more uniform than the initial states.

In this work we present results based on two modeling approaches. In the first part of the analysis we employ the simulation procedure of *Ben-Zion and Rice* [1993] to study the distribution of slip, the shape of rupture fronts, and the frequency-size (FS) and temporal statistics of earthquakes in a discrete cellular model of the central San Andreas fault (SAF). The use of a discrete cellular model is motivated by numerous observations which indicate that crustal rocks are massively fractured and fault zone geometry is highly irregular. Examples include interevent distance statistics of earthquakes [*Kagan*, 1991], profilometry measurements along exhumed fault surfaces [*Power et al.*, 1988; *Power and Tullis*, 1991], characterization of mapped SAF traces [*Aviles et al.*, 1987; *Okubo and Aki*, 1987], and analysis of geophysical logs from the 3.5 km deep Cajon Pass borehole [*Leary*, 1991]. In addition, elementary considerations based on fracture mechanics theory and simulation results from *Rice* [1993] and the second analysis section of the present work indicate that strong fault heterogeneities, acting as barriers, are necessary for the arrest (typically involving the resisting of large rupture-front stresses) of earthquakes of various sizes. Such barriers are presumably supplied by fault bends, forks and stepovers, complex fault walls topography, and/or complex pore pressure variations, and they can divide a fault system into numerous quasi-independent segments. In the presence of geometrical irregularities and other fault zone barriers, the propagation of fault instabilities beyond segment borders often involves stresses that are operating at finite distances from the rupture front, where slip can nucleate at weaker noncontiguous locations (e.g., as modeled by *Harris and Day* [1993] for rupture through fault stepovers). An elementary unit of such finite across-barrier distances is represented by the size of the numerical cells (a few hundreds of meters) used in our discrete cellular fault model. We note that while the discrete cells may model successfully some aspects of geometrically disconnected fault segments, they do not account for the deformation occurring between the segments and may thus neglect important features of foreshock and aftershock occurrence.

We assume that earthquake processes are nonergodic on a timescale of a few thousands of years. That is, over such periods, temporal sequences of earthquakes from given regions are not statistically equivalent among themselves, nor are they statistically equivalent to spatial ensembles of earthquakes occurring in different seismic zones. This is motivated by the fact that different crustal regions maintain distinct physical properties (e.g., distributions of cracks, pore pressure, fault lithology, stepovers, bends, depth of seismogenic zone) over similar and larger timescales. We thus study the evolution of stress and slip along different classes of heterogeneous fault systems, using property distributions that are characterized by different ranges of size scales. The mode of loading and the model properties (geometry, static and kinetic frictions) are kept constant in time; we assume that, on the average, these do not change significantly during a few earthquake cycles. On the other hand, the models have many quasi-independent segments, and the assumed (discontinuous) stress-slip relation is strongly nonlinear. Thus the simulated fault responses fall on a middle ground between the extreme behaviors of purely chaotic and purely predictable systems. All examined model realizations show nonrepeating sequences of events; however, the times of occurrence of the large model earthquakes have higher degrees of periodicity than that of a random Poisson sequence. This is more pronounced in models with relatively simple distributions of properties; as the distribution increases in complexity, with large property fluctuations extending over broader range of size scales, the times of occurrence of the large events become more irregular.

The simulations indicate that when a fault system is characterized by heterogeneities spanning a narrow range of size scales (e.g., a set of more-or-less uniformly spaced en echelon faults), self-similar frequency-size statistics of earthquakes can exist only up to a critical rupture area, the size of which may be used to estimate the dominant length scale (cell size in our discrete models) of the heterogeneities. In such systems the rates of occurrence of intermediate and large size (characteristic?) earthquakes are enhanced with respect to the self-similar power law distributions of small events. If a system belonging to this class is further characterized by a coherent tectonic brittle zone with more-or-less uniform dimensions, the enhancement of FS statistics beyond the critical event leads to local maxima, the observation of which may be used to infer the large-scale tectonic dimensions (width of the seismogenic layer or length of a fault segment bounded by barriers). Otherwise, the enhancement of seismicity beyond the critical event is spread and does not produce clear local maxima. A separate class of segmented fault systems is one characterized by heterogeneities spanning a broad range of size scales. In such systems, the scaling power law regime of seismicity extends to large events, and the FS statistics are approximately self-similar over the entire magnitude range. Recent observations of FS statistics of earthquakes along faults in southern California [*Wesnousky*, 1994] suggest that the combined San Jacinto fault zone belongs to the latter class of faults, while the various segments of the San Jacinto fault system and the Whittier-Elsinore, Garlock, and San Andreas faults belong to

the former. Other observations of FS statistics showing features of the first class of faults (narrow self-similar range, local maxima) are given by *Singh et al.* [1983], *Schwartz and Coppersmith* [1984], *Main and Burton* [1984, 1989], *Davison and Scholz* [1985], *Main* [1987], and *Trifu and Radulian* [1991]. (However, see *Kagan* [1993] for a discussion on possible biases and other problems in such data sets.)

In the second part of the analysis we use the simulation procedure of *Rice* [1993] to study the distribution of slip along a fault governed by rate- and state-dependent friction and subjected to various assumed distributions of pore pressure. Our aim is to use the more rigorous constitutive framework to learn what types of property heterogeneity on a smooth fault can induce responses similar to observations and those generated by our discrete cellular models. As in the work by *Rice* [1993], all cases calculated with cell size small enough to properly represent the underlying continuum model lead to periodic large earthquakes, although we note that the use of different friction laws may lead to aperiodic recurrence. A very strong pore pressure heterogeneity is needed to simulate in these models even a modest amount of complexity. This suggests that pore pressure variations in fault zone rocks are not the main mechanism responsible for the observed complex patterns of seismic slip, unless processes such as those proposed by *Byerlee* [1993], *Sleep and Blanpied* [1992], and *Sleep* [this issue] create fault zone compartments with extreme pressure variations capable of stopping seismic ruptures of various size. Also in agreement with *Rice* [1993], calculations done with strongly oversized cells, so that the model is effectively discrete, show features resembling the response of the discrete cellular model examined in the first part of the analysis and observed seismic behavior. The results of the second analysis section support the hypothesis that discrete fault models, accounting for 3-D continuum elasticity, may provide a valid approximate representation of fault zones having geometric disorder characterized by size scales much larger than the nucleation size of slip instabilities.

The simulations of *Rice* [1993], *Ben-Zion and Rice* [1993], and the present work show irregular sequence of earthquakes and a great diversity in the failure mechanism of model events. The results indicate that strategies for short-term earthquake prediction can not be based on simple repetitive precursory patterns such as accelerated microearthquake slip, although such occurs before some of the large model events. The studies suggest that the spatio-temporal complexity of fault slip is related to strong fault zone heterogeneities, probably due to geometric irregularities and perhaps also extreme pore pressure fluctuations, capable of stopping ruptures of various sizes. We note that our results are based on simulations with only approximate inclusion (e.g., by radiation damping term or allowance for dynamic overshoot) of elastodynamic effects.

Analysis

Modeling Based on Discrete Cellular Fault Zone Structure

Figure 1 shows a model of the central SAF from *Ben-Zion and Rice* [1993]. The model consists of an elastic half-space with a vertical half-plane fault; the half-space has a 17.5-km-thick brittle upper crust over a lower crust and upper mantle region where stable sliding occurs. The fault region in the upper crust contains large earthquake patches (regions I and IV) representing the rupture zones of the 1857 and 1906 *M*8 events. On these patches we impose a staircase slip history with a recurrence time of 150 years. Everywhere along the lower crust and upper mantle (region V) and in the upper crust fault segment that is distant from Gold Hill (GH) by more than 70 km (region III) we impose slip at a constant plate rate V_{pl} = 35 mm/yr. The upper crust fault segment $0 \le x \le 70$ km, $0 \le z \le 17.5$ km (region II) comprises a computational grid where space and time evolution of stress and displacement fields due to the imposed slip are calculated using a variant of static/dynamic friction law and 3-D continuum elasticity. Different distributions of stress drops on failing

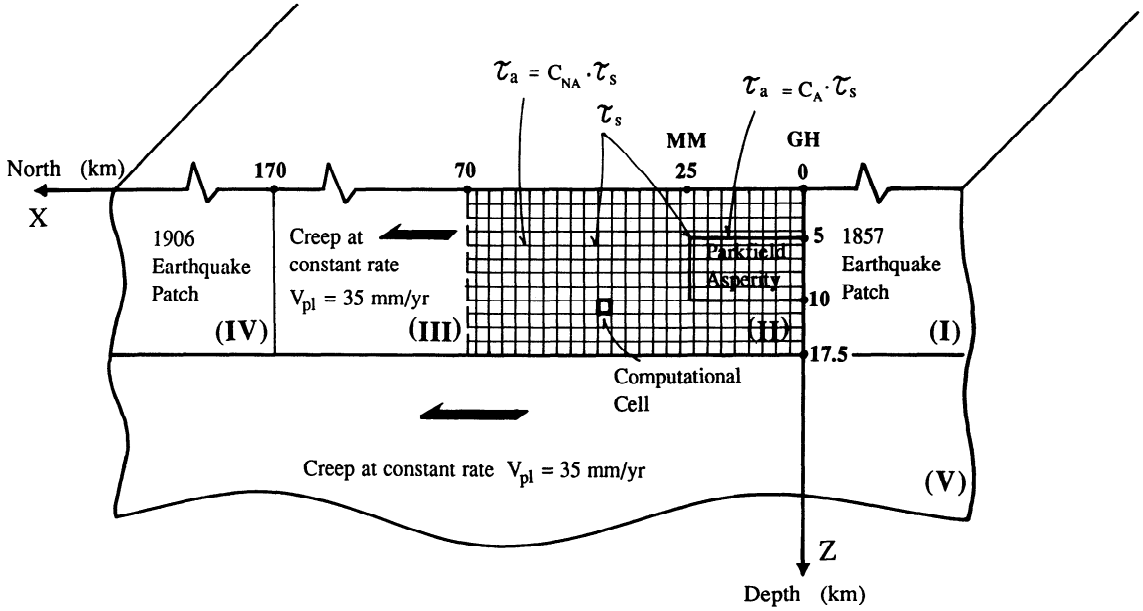

Figure 1. A model for the central San Andreas fault (SAF). τ_s is static strength assumed uniform over the computational region, τ_a is arrest stress, C_A and $C_{NA} \ge C_A$ are numerical coefficients, GH and MM mark approximate positions of Gold Hill and Middle Mountain.

computational cells are used to model fault regions with variable frictional properties. One model configuration, shown explicitly in Figure 1, is that of a fault containing a large rectangular region having different properties than the rest of the fault and designated as the "Parkfield asperity."

Consider a failure process involving a fault segment represented by a single cell of the computational grid. When the stress τ on the fault segment (precisely, at the cell center) reaches a static strength τ_s, failure occurs and the entire segment slips uniformly at a dynamic stress level $\tau = \tau_d$ ($<\tau_s$) until the rupture is blocked by the segment borders. Then, slip on the cell is brought to a halt, leaving on the failed segment an arrest stress τ_a ($<\tau_d$). If the stress transferred from the failed segment increases the stress at other fault regions to their failure thresholds those regions fail, causing additional stress transfers which, in turn, may induce or reinduce more slip events. We assume that reinitiation of slip on an already failed cell occurs when $\tau \geq \tau_d$ there. Thus τ_s is the failure strength of a segment which has not yet slipped in a composite event, τ_d is the failure strength of a segment which has slipped in an earlier subevent, and τ_a is the stress remaining on a cell just after it has slipped and before stress transfers from other segments failing at the same time have occurred. The static strength, dynamic strength, and arrest stress are related to each other as $(\tau_s - \tau_a)/(\tau_s - \tau_d) = D$, where D, set in this work to 1.25, is a dynamical overshoot coefficient. The difference $\tau(i, j) - \tau_a(i, j)$ gives a transient stress drop on cell (i, j) during a composite failure episode, where i and j are cell indexes along the horizontal and vertical directions, respectively, and $\tau(i, j)$ is the stress just before failure. The final stress drop on cell (i, j) is usually less than $\tau(i, j) - \tau_a(i, j)$ due to subsequent failures of other cells but is always greater or equal to $\tau(i, j) - \tau_d(i, j)$.

The evolution of stress and displacement fields in the computational region is calculated using the procedure outlined by *Ben-Zion and Rice* [1993]. The stress transfer due to incremental tectonic loadings and failing grid cells is computed by a discretized form of a boundary integral equation, based on the static solution of *Chinnery* [1963] for dislocations in a 3-D elastic half-space. The results are independent of the absolute values of τ_s, τ_d, and τ_a, and only stress drops enter model calculations. We model spatial differences in fault properties by assigning different levels of $\tau_s - \tau_a$ to different fault regions. As in the work by *Ben-Zion and Rice* [1993], the static strength is kept constant (for a given model realization), and spatial differences in stress drops are modeled via corresponding spatial differences of τ_a. To prevent confusion, we emphasize that our model makes no assumptions on the absolute strength of faults; all the analysis results are invariant with respect to constant shifts in the level of the assumed stresses. Also, one may reasonably expect that long-term earthquake statistics, for a given distribution of $\tau_s - \tau_a$, are independent of the individual distribution of τ_s or τ_a. The simulation procedure generates large ruptures as aggregates of small subevents on quasi-independent fault segments, on each of which there are initiation, propagation and arrest events, and possible reinitiations or repeated reinitiations. The most important model parameters are the number and size of grid cells, the distributions of $\tau_s - \tau_a$, and the recurrence interval and failure timing of the 1857 and 1906 patches.

The calculations are done using 128 × 32 = 4096 square cells having a dimension of about 550 m. This is close to the size of the regions (dimension of about 200 m) that contain clusters of repeated microearthquakes at Parkfield [*Nadeau et al.*, 1994; *Johnson and McEvilly*, this issue]. We begin all simulations with a 150 years of model-conditioning analysis during which the 1857 and 1906 earthquake patches (regions I and IV in Figure 1) are locked; the stably sliding zones (regions III and V in Figure 1) move by the amount $V_{pl}\, t$ = 35 mm/yr × 150 years = 5.25 m; and the stress-slip responses

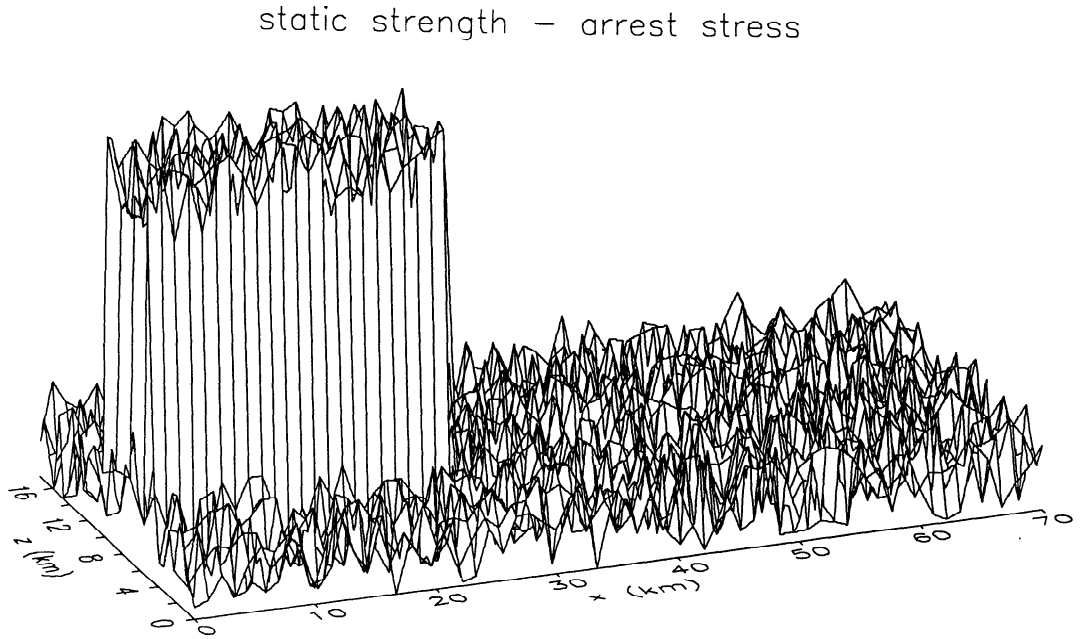

Figure 2a. Case 2 of text. Assumed stress drops representing a fault with an explicit Parkfield-type asperity and uncorrelated random property variations. The static strength is τ_S = 60 bars. In the asperity region the average arrest stress is $\tau_a = 0.1\tau_S$. In the nonasperity region the average arrest stress is $\tau_a = 0.8\tau_S$. The amplitude of the random fluctuations is $0.1\tau_S$.

along the computational grid (region II) are calculated as discussed above. The fault configuration at the end of the model-conditioning period provides nonzero heterogeneous initial states of stress and displacement for the continuing analysis. At $t = 0^+$ year into the analyzed earthquake cycle we impose 5.25 m of right-lateral slip (equal to the accumulated plate motion in 150 years) on the 1857 and 1906 earthquake patches. For simplicity, both earthquake patches are moved simultaneously. We note that in the present modeling the computational grid is largely "shielded" from the 1906 earthquake patch by the presence of the uniformly sliding region III.

We consider five cases of prescribed property distributions. (1) The first case is a fault with a large rectangular model Parkfield asperity. We assume that the static strength is τ_s = 40 bars (4 MPa). In the region $0 \le x \le 25$ km, 5 km $\le z \le 10$ km (Parkfield asperity), $\tau_a = 0.1\tau_s$. In the other fault regions, $\tau_a = 0.9\tau_s$. The spatial extent of the model asperity is compatible with geodetic data [e.g., *Harris and Segall*, 1987] and microearthquake distribution [e.g., *Malin et al.*, 1989; *Johnson and McEvilly*, this issue] along the central SAF. The assumption of different stress drops in the asperity and nonasperity regions is compatible with the observations of *O'Neill* [1984] and *Malin et al.* [1989]. (2) The second case is another example of an explicit model Parkfield asperity (Figure 2a). In the region $0 \le x \le 25$ km, 5 km $\le z \le 10$ km, $\tau_a = 0.1\tau_s \pm 0.1\tau_s$ uncorrelated random fluctuations. In the other fault regions, $\tau_a = 0.8\tau_s \pm 0.1\tau_s$ uncorrelated random fluctuations. To increase the model stress drops, we use here a static strength τ_s = 60 bars (see discussion below on the effects of model stress drops). (3) The third case is a fault with uniform distributions τ_s = 60 bars and $\tau_a = 0.8\tau_s$. (4) The fourth case is a fault with a fractal property distribution (Figure 2b). The static stress is τ_s = 60 bars. The arrest stress is $\tau_a = f\tau_s$, where f is taken from a fractal distribution generated by a program outlined by *Brown* [1995]. The distribution is characterized by a fractal dimension 2.3, mean value 0.5, and standard deviation 0.2. (5) The fifth case is a fault consisting of low stress drop segments of variable size, separated by high stress drop boundaries (Figure 2c). Cells along the free surface are selected randomly with a probability of 1/5. The selected cells initiate one-cell-thick segment boundaries; these are extended to depth by 2-D random walks. In cells belonging to segment boundaries, $\tau_a = 0.1\tau_s$. In other cells, $\tau_a = 0.9\tau_s$. The static strength is τ_s = 100 bars. This case may be taken as an example of a fault with multi-size-scale structural heterogeneities along strike, with the high stress drop boundaries representing stepovers of the fault plane. Alternatively, the low stress drop regions may represent fault sections with high fluid pressure [*Byerlee*, 1990, 1993; *Rice*, 1992], while the high stress drop regions may correspond to high-permeability segments with hydrostatic pore pressure. It is interesting to compare the fault properties of case 5 with the overpressurized fault zone compartments separated by impermeable seals of *Byerlee* [1993]. In the model of *Byerlee* [1993] the overpressurized regions are approximately equidimensional and the seals extend along both the horizontal and vertical directions. The fault zone structure of case 5, on the other hand, contains a range of size scales, and the high stress drop boundaries are predominantly vertical. The dominant direction of segment boundaries is not important for our results; however, as discussed below, the range of size scales in the assumed fault zone properties is a key model attribute.

Figure 3 shows time sequences of model earthquakes with magnitude $M \ge 5.5$ during 100 years for the five considered cases. Earthquake magnitudes are calculated using the relation $M = (2/3)\log(P) + 3.6$, where P is potency (the integral of slip over the rupture area) in square kilometers times centimeters. The above expression follows from the moment-magnitude

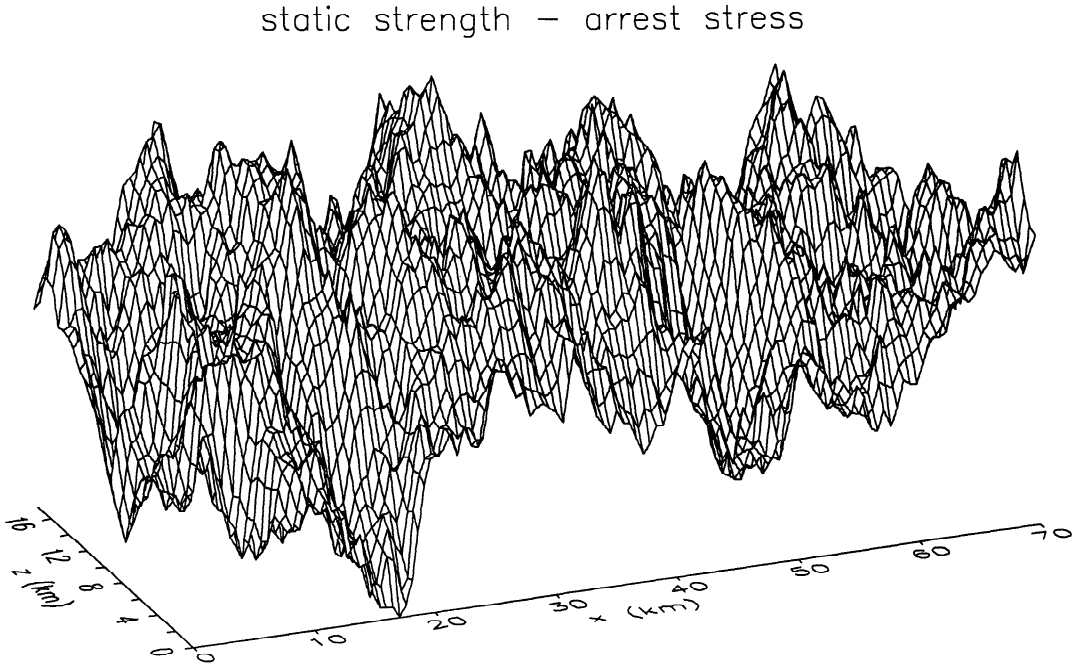

Figure 2b. Case 4 of text. Assumed stress drops representing a fault with a fractal property distribution. The static strength is τ_s = 60 bars. The arrest stress is $\tau_a = f\tau_s$, where f is taken from a fractal distribution characterized by a fractal dimension 2.3, mean value 0.5, and standard deviation 0.2.

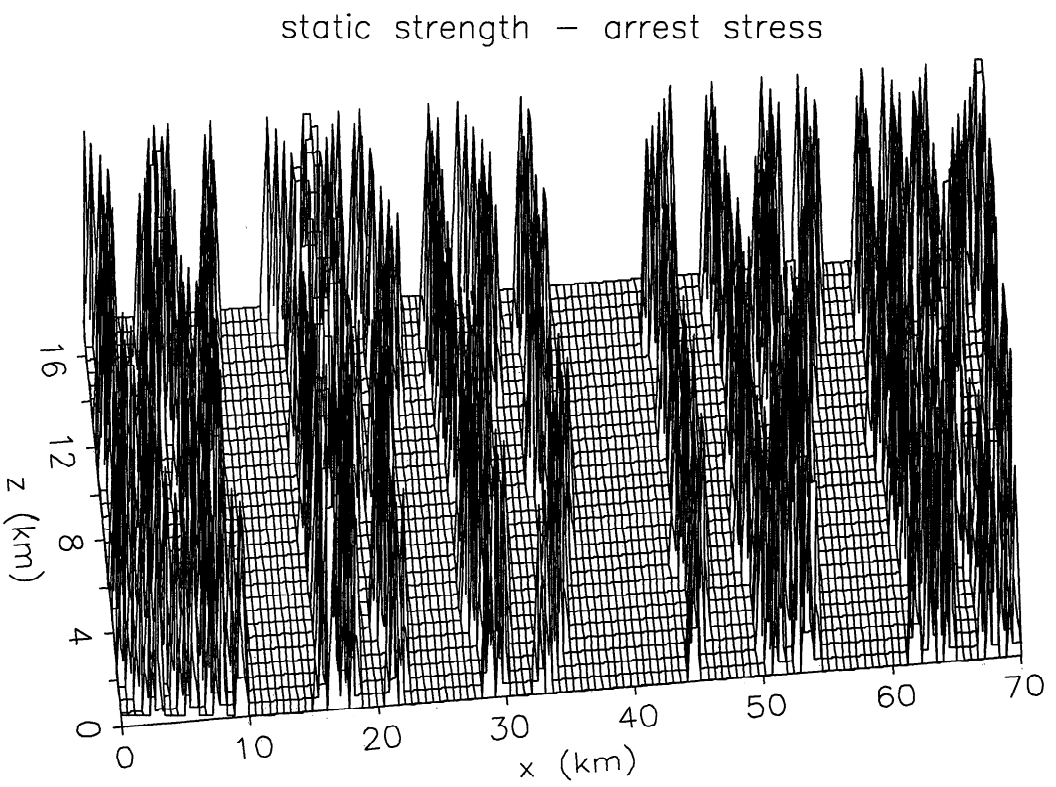

Figure 2c. Case 5 of text. Assumed stress drops representing a fault with multi-size-scale heterogeneities. The fault consists of low stress drop segments of variable size separated by high stress drop boundaries. In cells belonging to segment boundaries, $\tau_a = 0.1\tau_s$. In other cells, $\tau_a = 0.9\tau_s$. The static strength is $\tau_s = 100$ bars. See text for more explanation.

relation of *Hanks and Kanamori* [1979] upon using a nominal rigidity of 30 GPa (3×10^{11} dyn/cm^2) and accounting for the change in units. The results of Figure 3 illustrate a few general characteristics of the various model realizations. The magnitude of model earthquakes increases with the average stress drop on failing cells and the size of the rupture area. Table 1 lists average values of $\tau_s - \tau_a$ over the computational grid for the various model realizations. These values represent approximately the average stress drops during moderate and large model earthquakes. The model realizations cases 1 and 2 have two size scales that can affect the extent of rupture areas associated with moderate and large events. These are the size of the Parkfield asperity and the complementary remainder area of the computational grid. In cases 3 and 4 there are no intermediate size scales between cell size and the size of the computational grid, while in case 5 there are many such intermediate size scales. Thus, in cases 1 and 2 the moderate and large events occur predominantly in two magnitude ranges associated with the two intermediate areal size scales of the models, while in cases 3-5 the distributions of event sizes are broader.

In case 5, where the fault contains low stress drop regions of various sizes separated by high stress drop barriers, ruptures are arrested with high probability before they can grow to a large size (i.e., a size of the order of the computational grid). Thus, although the average stress drop over model 5 is relatively large, the size and, consequently, interevent time interval of most $M \geq 5.5$ events are, in that case, small in comparison to those of the other model realizations. In case 4, where the property distribution does not have any intermediate size scale and the average stress drop is large, the situation is opposite. Here, the size and interevent time interval of most $M \geq 5.5$ events are larger than in any of the models. In cases 1-3, with a few intermediate size scales (for cases 1-2) and relatively low average stress drops, the size and interevent time of most moderate and large earthquakes are between those of cases 4 and 5.

The earthquake sequences of Figure 3 show various degrees of periodicity. Table 1 gives the mean μ, standard deviation σ, and ratio μ/σ of time intervals between model earthquakes in the magnitude ranges $M \geq 5.5$ and $M \geq 6.0$. As pointed out by, e.g., *Kagan and Jackson* [1991], for a random Poisson sequence the ratio μ/σ is equal to one, while for quasi-periodic and clustered sequences the ratios are greater and smaller than one, respectively. The ratios of μ/σ listed in Table 1 indicate that the moderate and large earthquakes of all model realizations are quasi-periodic; the degree of periodicity is seen to increase with earthquake size and to decrease with model complexity. *Kagan and Jackson* [1991] found that strong events in global and regional (central California) earthquake catalogs are clustered rather than quasi-periodic. However, the simulations of the present work are done for a single (the central San Andreas) fault and not for a large collection of faults. As shown in Table 2 of *Ben-Zion et al.* [1993], observed time intervals between the $M \approx 6$ Parkfield earthquakes of the last century, as well as calculated (layered elastic/viscoelastic) model slip deficits between the events, have ratios μ/σ in the range 2.75-3.20. These values are similar to those characterizing the large event sequences in

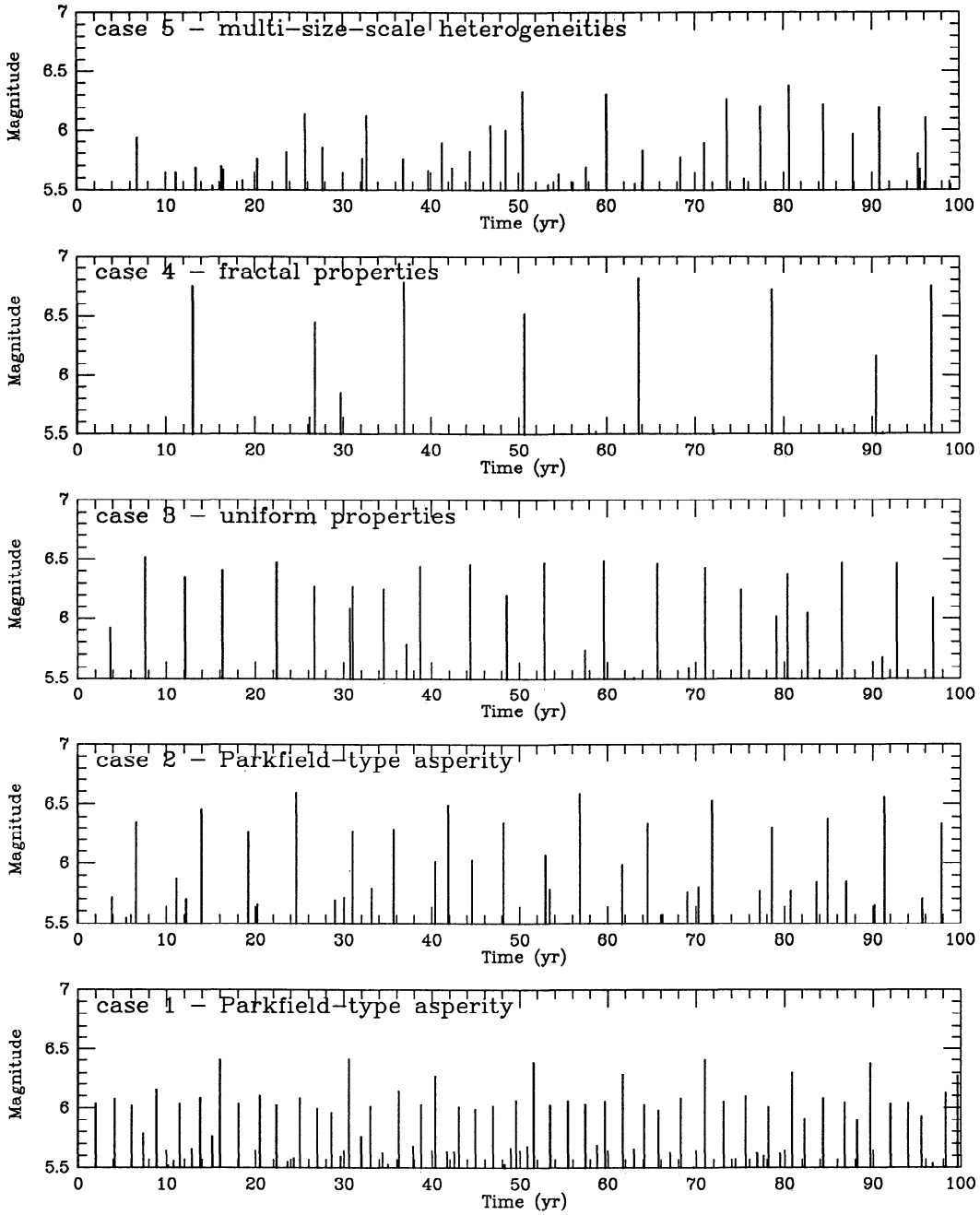

Figure 3. Moderate and large earthquakes in cellular model realizations. See text and Figure 2 for fault properties in cases 1-5.

cases 1-2 (a fault with an explicit Parkfield asperity) and to a lesser extent also in case 3 (a uniform fault).

While the results of Figure 3 and Table 1 indicate that the large model earthquakes are quasi-periodic, the nature of the large events is highly variable and the models generate nonrepeating chaotic sequences. This is illustrated in Figure 4 where we show, for the simple case 1, cumulative rupture area as a function of time along the asperity region $0 \le x \le 25$ km, 5 km $\le z \le$ 10 km. We note that the character of the large events varies from one earthquake to the other. The event at about 180 years is preceded by a period of gradual rupture formation; the events at about 190, 220, and 240 years are abrupt; the events at about 210 and 230 years occur as swarms of smaller events or microearthquake slip; the events at about 200 and 260 years are preceded by "foreshocks"; and the event at about 280 years is followed by an "aftershock." The diversity in the failure mechanism of the model asperity may be a manifestation of the many paths toward a low energy state, available to a complex nonlinear many-degrees-of-freedom system. The results indicate that expectations for simple and regularly occurring diagnostic precursory patterns, such as accelerated microearthquake slip, are unrealistic; such patterns may occur before some failures, but they are not very indicative.

Figures 5a and 5b show time evolution of slip along the SAF at a depth of 8.75 km for cases 2 and 5 above. In Figure 5a

Table 1. Parameters of Moderate and Large Earthquakes in Cellular Fault Models

	$\langle\tau_s - \tau_a\rangle$, bars	$\mu(M \geq 5.5)$, years	$\sigma(M \geq 5.5)$, years	$\mu(M \geq 6)$, years	$\sigma(M \geq 6)$, years	$\mu/\sigma(M \geq 5.5)$	$\mu/\sigma(M \geq 6)$
Case 1 (Parkfield-type asperity)	7.23	1.38	0.53	2.55	0.83	2.63	3.07
Case 2 (Parkfield-type asperity)	16.24	2.47	1.48	5.70	2.07	1.67	2.74
Case 3 (uniform properties)	12.00	3.25	1.37	4.39	1.77	2.36	2.48
Case 4 (fractal properties)	33.16	5.76	4.09	9.36	4.38	1.41	2.14
Case 5 (multi-size-scale heterogeneities)	22.82	2.80	2.08	8.49	5.59	1.34	1.52

The $\langle\tau_s - \tau_a\rangle$ is average of static strength minus arrest stress over the computational grid; $\mu(M \geq A)$ and $\sigma(M \geq A)$ are, respectively, mean and standard deviations of time intervals between earthquakes with magnitudes $M \geq A$.

and in calculations corresponding to case 1 (not shown), where the assumed properties account explicitly for a large Parkfield asperity, slip in the region $0 \leq x \leq 25$ km is accommodated in the form of large steps separated by periods of little or no activity, while slip in the region $x > 25$ km is accommodated in a nearly continuous fashion. These results are compatible with geodetic data and earthquake distribution along the central SAF. On the other hand, in Figure 5b and in calculations corresponding to the property distributions 3 and 4 (not shown), time evolutions of slip in the region $0 \leq x \leq 25$ km are not clearly distinguishable from slip histories at other fault segments.

Figure 6a shows a typical example of a rupture area during a simulation corresponding to case 3 above. The results demonstrate that when the fault properties are smooth functions of space, the shape of the rupture front is also smooth. When, however, the fault properties vary rapidly in space, as in cases 1, 2, 4, and 5, the stress field along the rupture front is characterized by large spatial variations, and a typical shape of the rupture front is rough. This is illustrated in Figure 6b for the property distribution of case 5. The results of Figures 5 and 6 indicate that strong fault heterogeneity is required, at least in this type of modeling, for the generation of displacement fields compatible with geodetic and seismological observations and rough rupture fronts capable of radiating high-frequency seismic waves. There may also exist elastodynamic reasons for roughness of a rupture front. We note that discontinuous rupture areas like that of Figure 6b

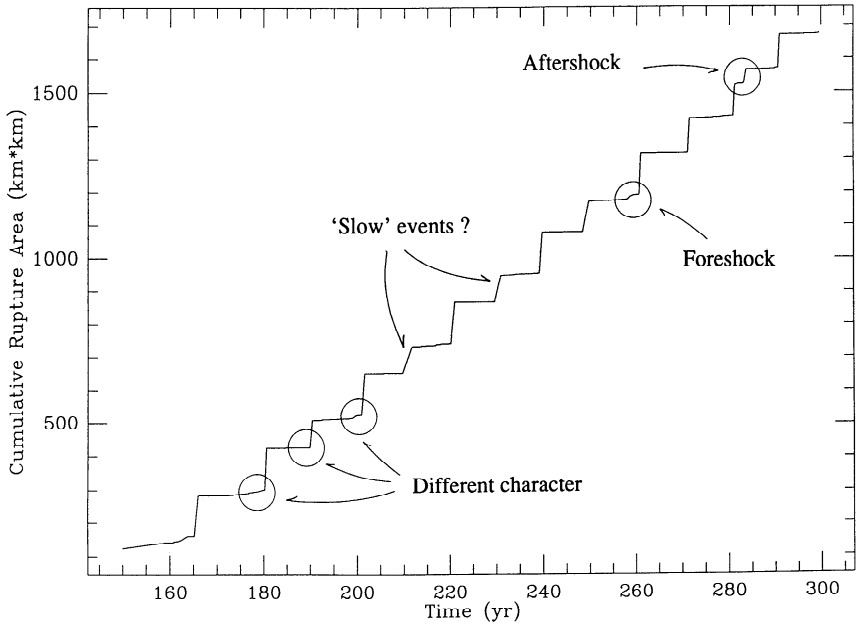

Figure 4. Cumulative rupture area at the Parkfield asperity region for case 1 of text. Note the diversity in the character of the large events.

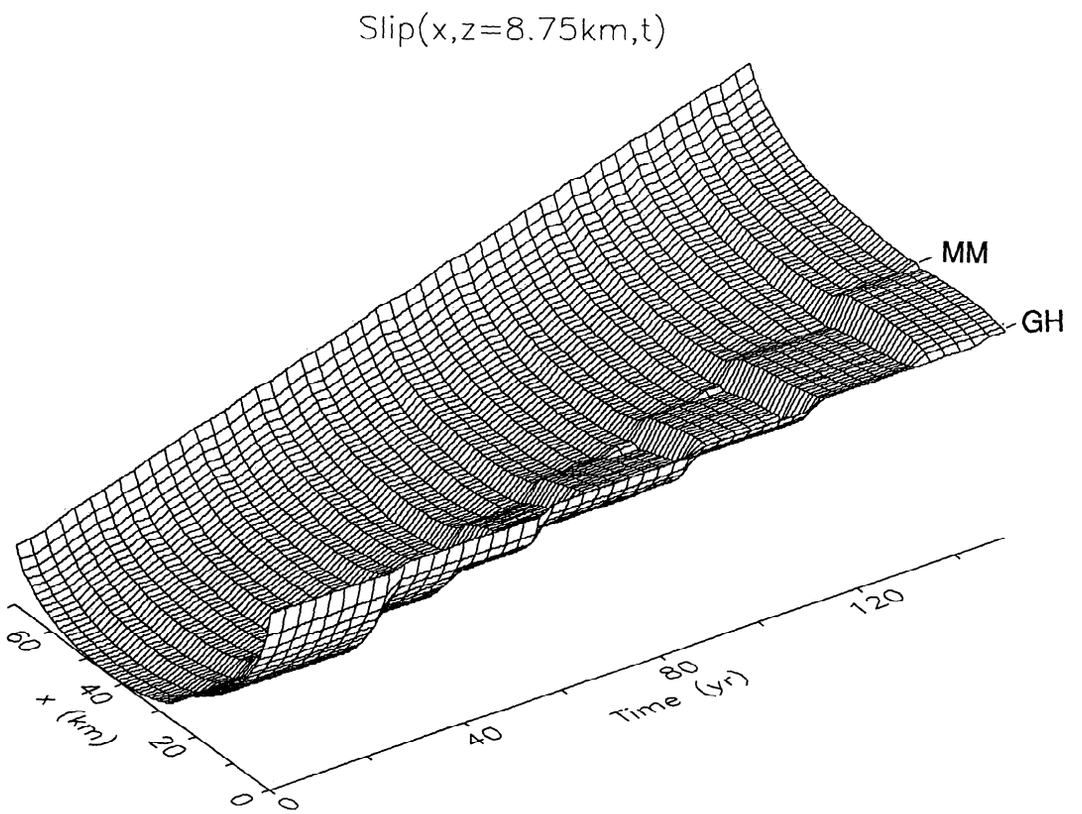

Figure 5a. Slip (normalized to the range 0-1) at a depth of 8.75 km as a function of distance along the SAF and time for the property distribution of Figure 2a (case 2 of text).

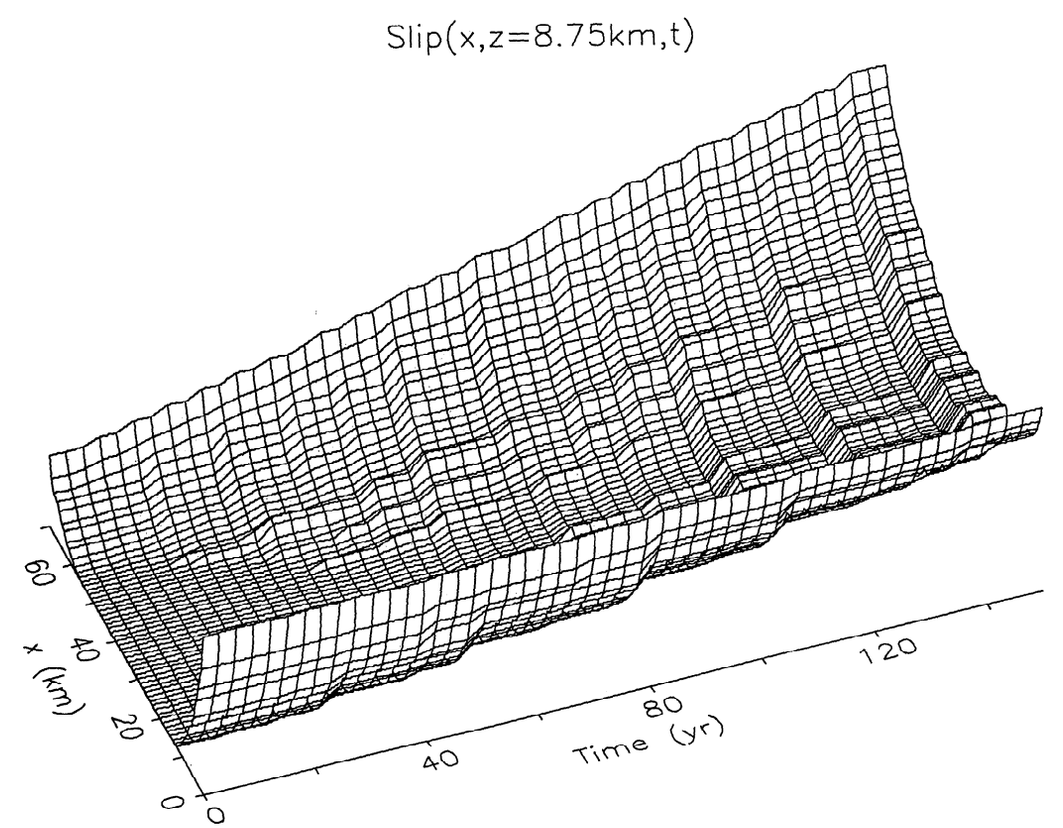

Figure 5b. Same as Figure 5a for the property distribution of Figure 2c (case 5 of text).

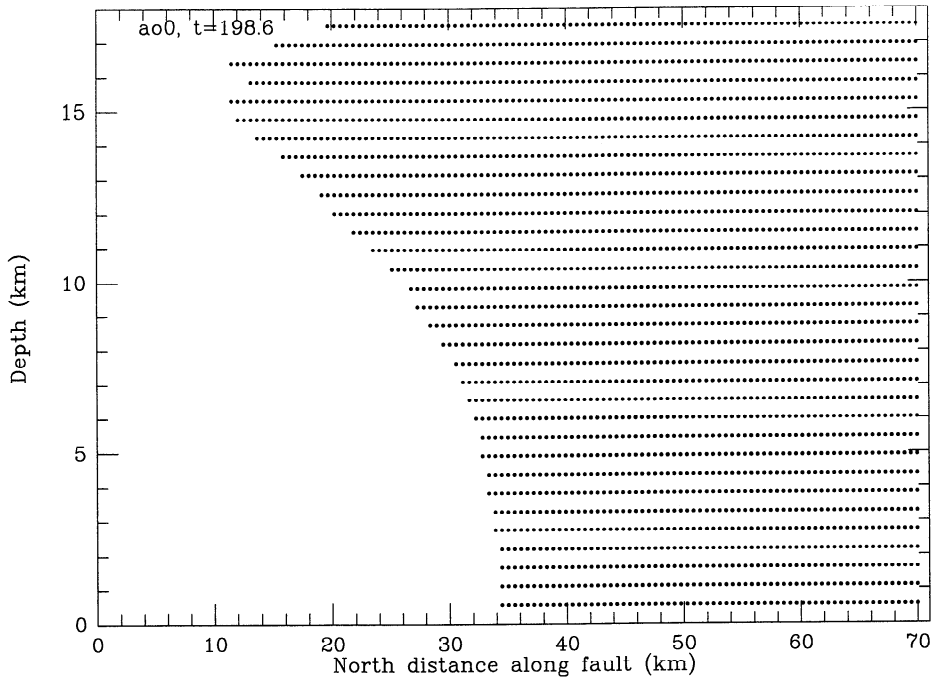

Figure 6a. Rupture area (dots) with a smooth front in simulation with uniform fault properties (case 3 of text).

are commonly simulated by the heterogeneous realizations of our cellular fault model, with stress redistributions during slip episodes governed by continuum elasticity. Such spatially discontinuous failure zones are not accounted for by cellular automata and block-spring simulations, where stress transfers occur only over a short range (typically over nearest neighbors).

Figure 7a shows cumulative frequency-size statistics of rupture area and earthquake magnitude in the computational grid $0 \le x \le 70$ km, $0 \le z \le 17.5$ km during 150 analysis years for the stress drop distribution of case 1. The units of rupture area are square kilometers; log = $\log_{10}$. The FS statistics are discussed with a reference to the Gutenberg-Richter power law distribution $N(S) = aS^b$. In cumulative statistics, $N(S)$ is the number of events with size, measured by magnitude M or rupture area A, larger than S; in noncumulative statistics, $N(S)$

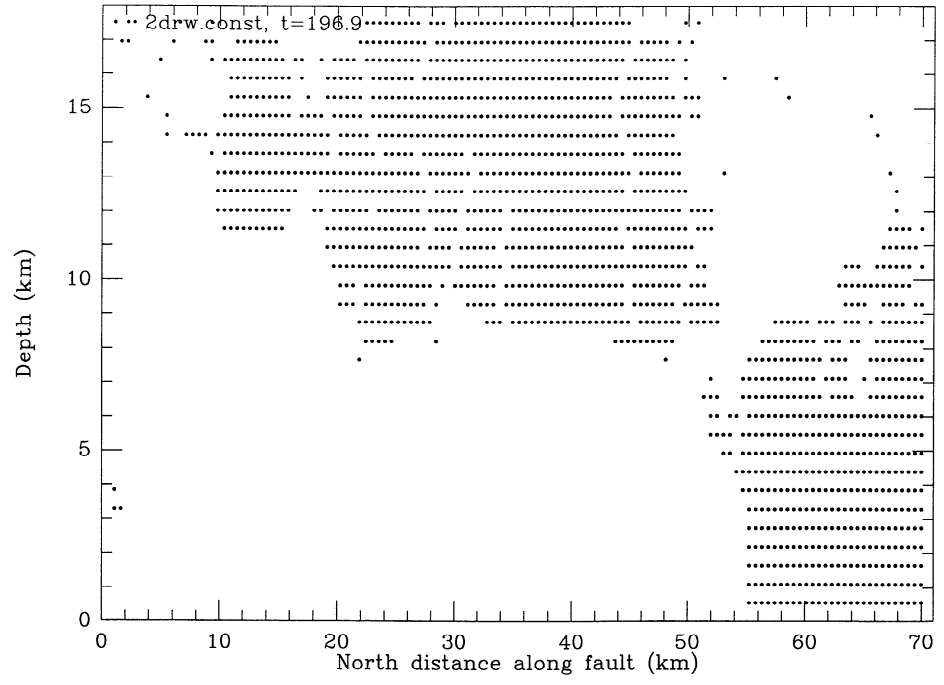

Figure 6b. Rupture area (dots) with a rough front in simulation with nonuniform fault properties (case 5 of text, Figure 2c). Note that the rupture area is discontinuous.

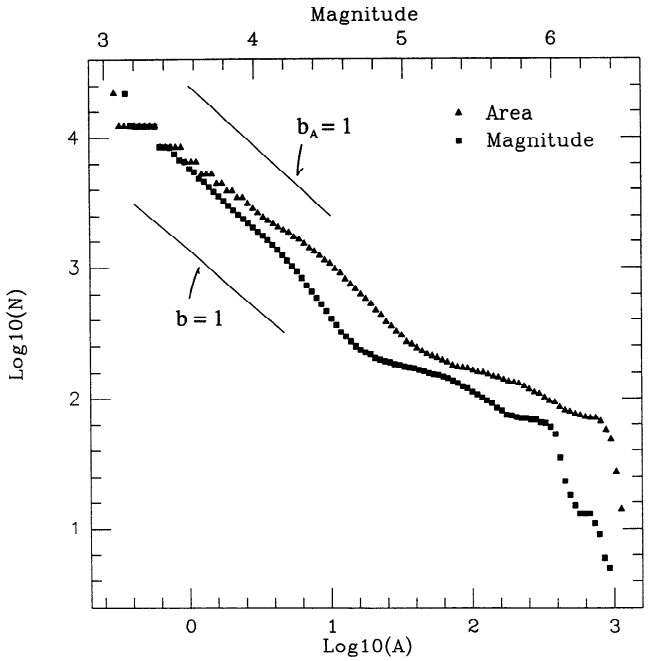

Figure 7a. Cumulative frequency-size (FS) statistics of earthquake magnitude (squares) and rupture area (triangles) during 150 analysis years in the computational grid for a stress drop distribution like in Figure 2a but without random fluctuations (case 1 of text), having two characteristic size scales (cell size and the size of the asperity). Units of rupture area are square kilometers.

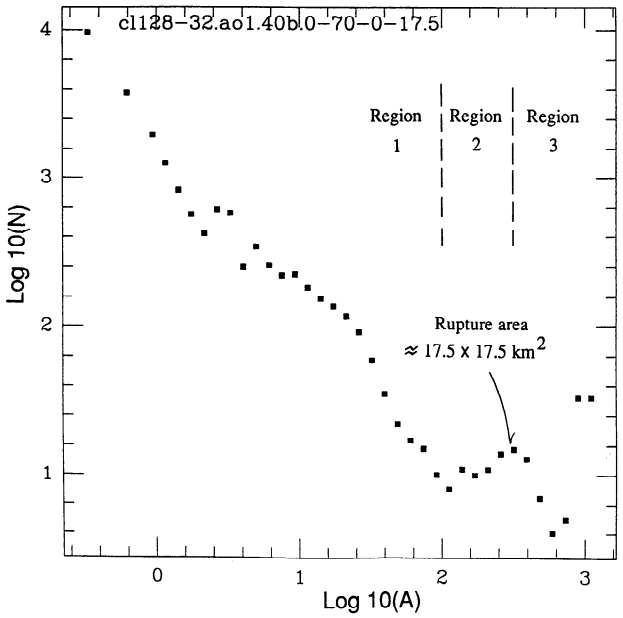

Figure 7b. Same as Figure 7a for noncumulative FS statistics of rupture area. Region 1 is a self-similar domain with $b_A \approx 1$; region 2 shows enhancement in frequency of intermediate size events with a peak at a rupture area having the dimension of the upper layer thickness; region 3 is a final steep decay ending with a peak for events the size of the computational grid.

is the number of events in a given interval around S. The constants a and b express the general level of seismic activity, and the relation between seismicity rates at different magnitude ranges, respectively; the exponent b (a slope in the log-log presentations of Figures 7-9) is commonly referred to as the b value. The FS statistics of Figure 7a show three clear event groups: small events characterized by $b \approx 1.2$ and $b_A \approx 1$ (b and b_A are b values based on earthquake magnitude and rupture area, respectively), intermediate size events having b, $b_A < 0.5$, and a final steep fall off. A region b, $b_A \approx 1$ is commonly observed and simulated, indicating that small events are self-similar. The intermediate region results from a supercritical rupture growth beyond a critical event size. This is better seen in Figure 7b where we show corresponding noncumulative FS statistics of rupture area. The small events fall more-or-less on a self-similar curve, but beyond a rupture area of about 80 km^2 events usually continue to grow to a size that is limited either by the upper layer thickness ($\approx$ 17.5 x 17.5 km^2) or the entire model dimensions ($\approx$ 70 x 17.5 km^2). As discussed by *Ben-Zion and Rice* [1993], the deviation of the simulated FS statistics from a power law (self-similar) distribution for events larger than a critical size is a direct consequence of continuum elasticity. More specifically, it is due to the fact that the stress concentrated in an elastic solid at the edge of an expanding rupture grows with the size of the failure zone. When the assumed fault properties are characterized, as in case 1, by a narrow range of size scales (representing, e.g., a narrow range of geometric disorder), the scaling of stress concentrations with the rupture area introduces a critical event size terminating the self-similar earthquake statistics. In such systems, events reaching the critical size become (on the average) unstoppable, and they continue to grow to a size limited by a characteristic system dimension. We note that the simulated FS statistics of Figure 7 are compatible with the observed Parkfield seismicity, where

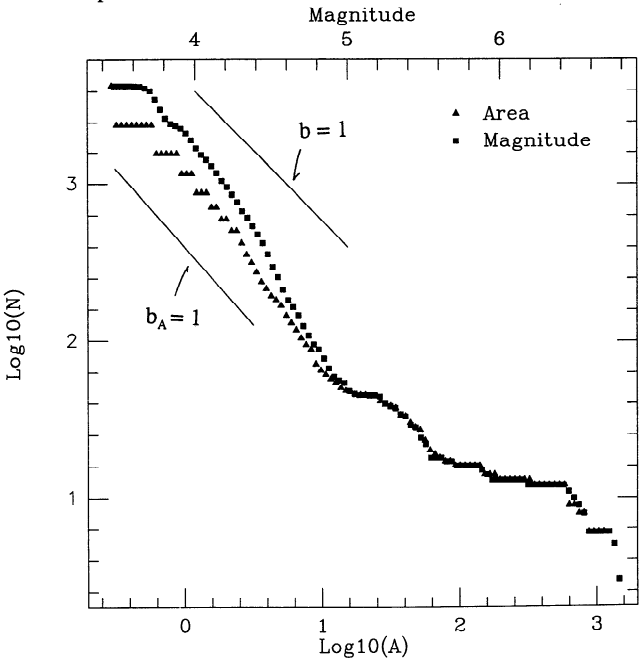

Figure 8a. Cumulative FS statistics of earthquake magnitude and rupture area during 150 analysis years in the computational grid for the fractal stress drop distribution of Figure 2b (case 4 of text), having a single characteristic size scale (cell size).

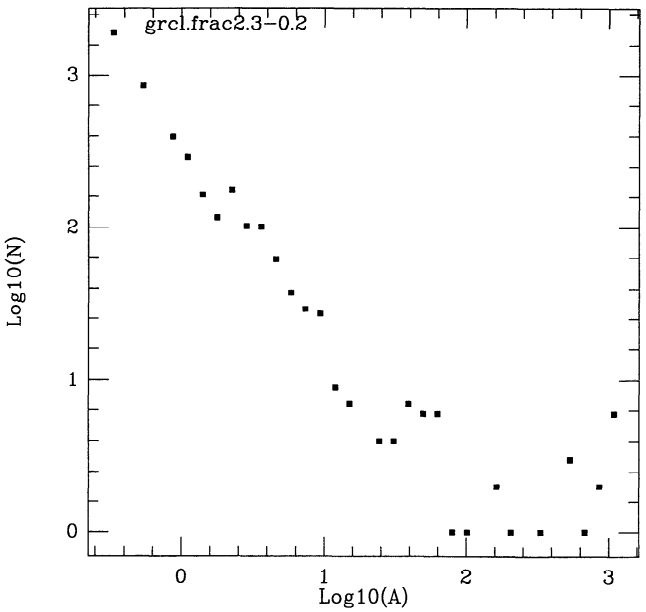

Figure 8b. Same as Figure 8a for noncumulative FS statistics of rupture area.

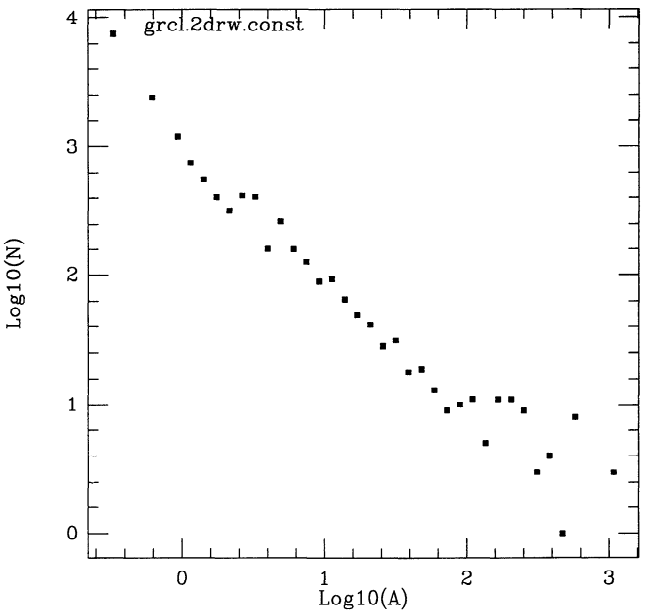

Figure 9b. Same as Figure 9a for noncumulative FS statistics of rupture area.

the rate of occurrence of five $M \approx 6$ Parkfield earthquakes in a century is strongly enhanced with respect to the self-similar distribution of small events [*Ben-Zion and Rice*, 1993].

The statistics of Figure 7 are generated by a model with a simple property distribution and two characteristic size scales, namely, the size of the computational cell and the size of the model asperity. Figures 8a and 8b show, respectively, cumulative and noncumulative FS statistics for the fractal property distribution of case 4 (Figure 2b). Since the property distribution, although more complex than the model leading to Figure 7, is characterized by a single size scale, the range of self-similar statistics in Figure 8 is terminated at a critical rupture area similar to that of Figure 7. However, the highly heterogeneous (fractal) property distribution in the model corresponding to Figure 8 simulates barriers that can stop events at various stages between the critical rupture area and the size of the computational grid. Thus the statistics of Figure 8 do not show the clear local maximum observed in Figure 7 for events with rupture area the size of the upper layer thickness. Instead, Figure 8 exhibits a general enhancement of seismicity beyond the critical rupture area and a single maximum for events the size of the whole system. Figures 9a and 9b show FS statistics for the property distribution of case 5, where the model represents low stress drop fault regions of variable size and high stress drop intervening barriers (Figure 2c). Here, the assumed fault properties are characterized by many size scales and, consequently, the range of self-similar FS statistics is broader than those of Figures 7 and 8. The average b and b_A values of the FS statistics in Figure 9 are about 1. We note that owing to the scaling of stress concentrations in elastic solid with rupture size, the rate of occurrence of intermediate and large size events in all of Figures 7-9 is enhanced with respect to self-similar lines defined (strictly) by small events, regardless of the shape of the simulated statistics.

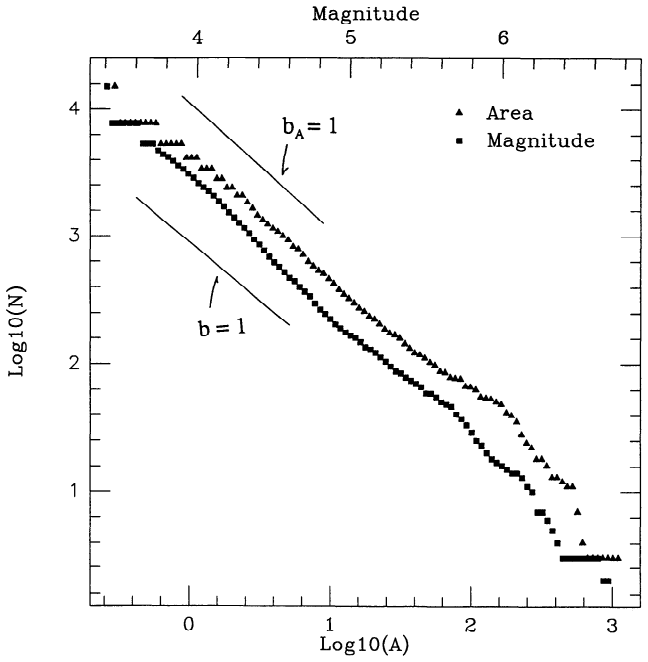

Figure 9a. Cumulative FS statistics of earthquake magnitude and rupture area during 150 analysis years in the computational grid for the stress drop distribution of Figure 2c (case 5 of text), having many size scales.

Modeling Based on Rate- and State-Dependent Friction With Nonzero Critical Slip Distance

We now describe some calculations in the framework of *Rice* [1993], with the aim of understanding how pore pressure distributions affect the earthquake cycle. Particularly, we examine how severe heterogeneities of pore pressure p may provide barriers adequate for stopping some ruptures and hence lead to a complex seismic response. The results are also used to examine possible connections between our discrete and continuum models. Such connections are important since the

numerical difficulties of accurately implementing the rate- and state-dependent friction are formidable, and thus it is advantageous to use simpler but compatible modeling approaches when appropriate. We limit attention here to distributions which are constant in time, and hence we do not evaluate such mechanisms as proposed by *Sibson* [1992], *Sleep and Blanpied* [1992], *Byerlee* [1993], and *Sleep* [this issue] where p is time dependent. Those mechanisms would require further model developments to represent, e.g., in the Sleep and Blanpied case, creep compaction, sealing off of permeability, and re-creation of porosity in rupture; and in the Byerlee case, pore fluid communication between fault compartments when a seal between them fails. All the reported results are based on analysis of the model shown in Figure 10, from *Rice* [1993], in which slip is imposed at V_{pl} = 35 mm/yr on the portion of a half-plane fault lying below 24 km in an otherwise homogeneous elastic half-space. Slip δ is calculated on the fault section between 0 and 24 km depth, and over that range a Ruina-Dieterich "slip" type of rate- and state-dependent constitutive law applies (later we note differences of results when the Dieterich-Ruina "slowness," or "ageing," law is used). Thus, over the depth range 0-24 km the shear stress τ satisfies

$$\tau / (\sigma_n - p) = f = f_o + a \ln [(d\delta / dt) / V_{pl}] + b\ \Psi$$

$$d\Psi / dt = - [(d\delta / dt) / L] \{\Psi + \ln [(d\delta / dt) / V_{pl}] \}. \quad (1)$$

Here f is a coefficient of friction, σ_n is the normal stress (equated to depth times 28 MPa/km), f_o is a constant which is irrelevant for the results to be shown, Ψ is a state variable, L is the critical slip distance for state evolution, and a and b are functions of temperature which are converted to functions of depth just as done by *Rice* [1993, Figure 3], based on the data of *Blanpied et al.* [1991] for granite under hydrothermal conditions. The assumed fault properties correspond to velocity strengthening regimes ($a > b$) for the depth sections 0-3 km and below 14 km, and a velocity weakening regime ($a < b$) elsewhere; in all calculated cases, $b - a$ = 0.004 over depths between about 4 and 13 km. The fault zone in the depth range 0-24 km is divided into numerical cells (Figure 10), and the system of equations is completed by writing from elastic theory

$$\tau_i = - \sum_j K_{ij} (\delta_j - V_{pl}\, t) - (\mu / 2c)\, d\delta_i / dt. \quad (2)$$

The subscripts in (2) refer to cell indices and K_{ij} is calculated from the *Chinnery* [1963] static solution as in the previous section. The last factor on the right side of (2) is a seismic radiation term with a damping coefficient $\mu/2c$, where μ is shear modulus of 30 GPa and c is shear wave speed of 3 km/s. As discussed by *Rice* [1993], this term is a feature of exact elastodynamics and it allows solutions to exist during instabilities, when purely quasi-static calculations lead to unbounded slip velocity. For that reason the procedure may be called quasi-dynamic to distinguish it from approaches like that of *Tse and Rice* [1986] which do not calculate solution details during dynamic instabilities.

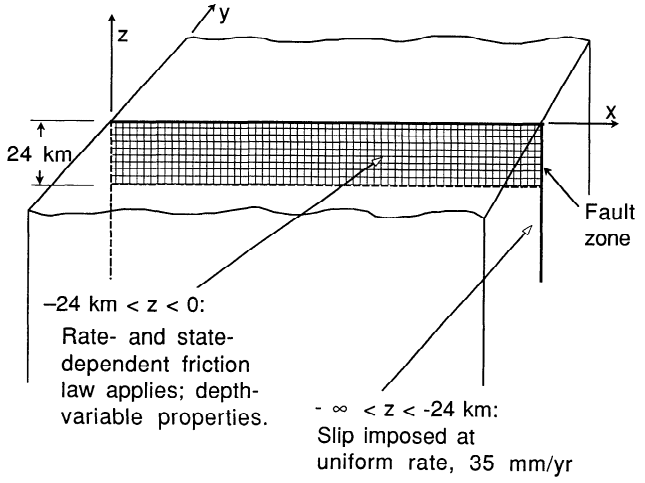

Figure 10. Elastic half-space with vertical half-plane strike slip fault. Slip imposed at 35 mm/yr below 24 km and calculated above 24 km according to rate- and state-dependent friction law, like in the work by *Rice* [1993]. The cases calculated in this work constrain slip to vary only with depth.

While Figure 10 suggests slip variation with depth and distance along strike, $\delta = \delta(x, z, t)$, we simplify matters here by constraining the slip to vary only with depth, i.e., $\delta = \delta(z, t)$. We discuss results of six calculations denoted as cases I to VI. Cases I to V are done with a cell height h that is small enough to assure that the calculations represent the continuum limit of the rate- and state-dependent friction law (1). Case VI illustrates results for an oversized h, i.e., a discrete system; as discussed in the introduction, the results for this case are very different in character from the results of cases I to V representing continuum systems. *Rice* [1993] defined a nucleation size h^* as the cell size h such that the "single-cell stiffness" $2\mu/\pi h$ becomes equal to the "critical spring stiffness" $(b - a)(\sigma_n - p) / L$; the equality marks a border between stable and unstable sliding for velocity weakening behavior of the adopted friction law.

In cases I to V we use 512 cells through the 24 km thickness, so that h = 0.047 km. The critical slip distance L is variable from cell to cell, but it is never smaller than 1 mm. In velocity weakening regions, L is chosen larger as necessary to make the local value of $h^* = 2L\,\mu/\pi\,(b - a)(\sigma_n - p)$ coincide with $8h$ = 0.375 km. More specifically, in cases I to V, L/mm = max [1, 19.6 $(b - a)(\sigma_n - p)$ / MPa]. In contrast, for case VI we take 64 cells through the thickness, so that h = 0.375 km, and we choose L so that in velocity weakening regions $h^* = h/4$, unless such requires an L smaller than 1 mm (this is again the minimum allowed value). Since the nucleation size in case VI is much smaller than cell size, the corresponding model behaves as an inherently discrete system with response features comparable to those of our cellular model having the simplified static/kinetic friction law and L = 0.

Figure 11 shows various pore pressure distributions used in the following calculations. The thin line in each of the four panels corresponds to a hydrostatic pore pressure (equal to depth times 10 MPa/km). The first example, designated as case I, simply assumes p is hydrostatic. This case, like all other calculated examples except case VI, leads to a periodic slip history. This is shown in Figure 12a where we plot slip versus depth; slip curves are drawn every 5 years and the total 14000 mm range of the slip axis corresponds to 400 years at 35 mm/yr. The recurrence interval for this case is about 140 years.

Case II involves the pore pressure distribution of Figure 11a; this consists of a hydrostatic pressure gradient above and below 8 km, a depth where a severe pressure step elevates p to

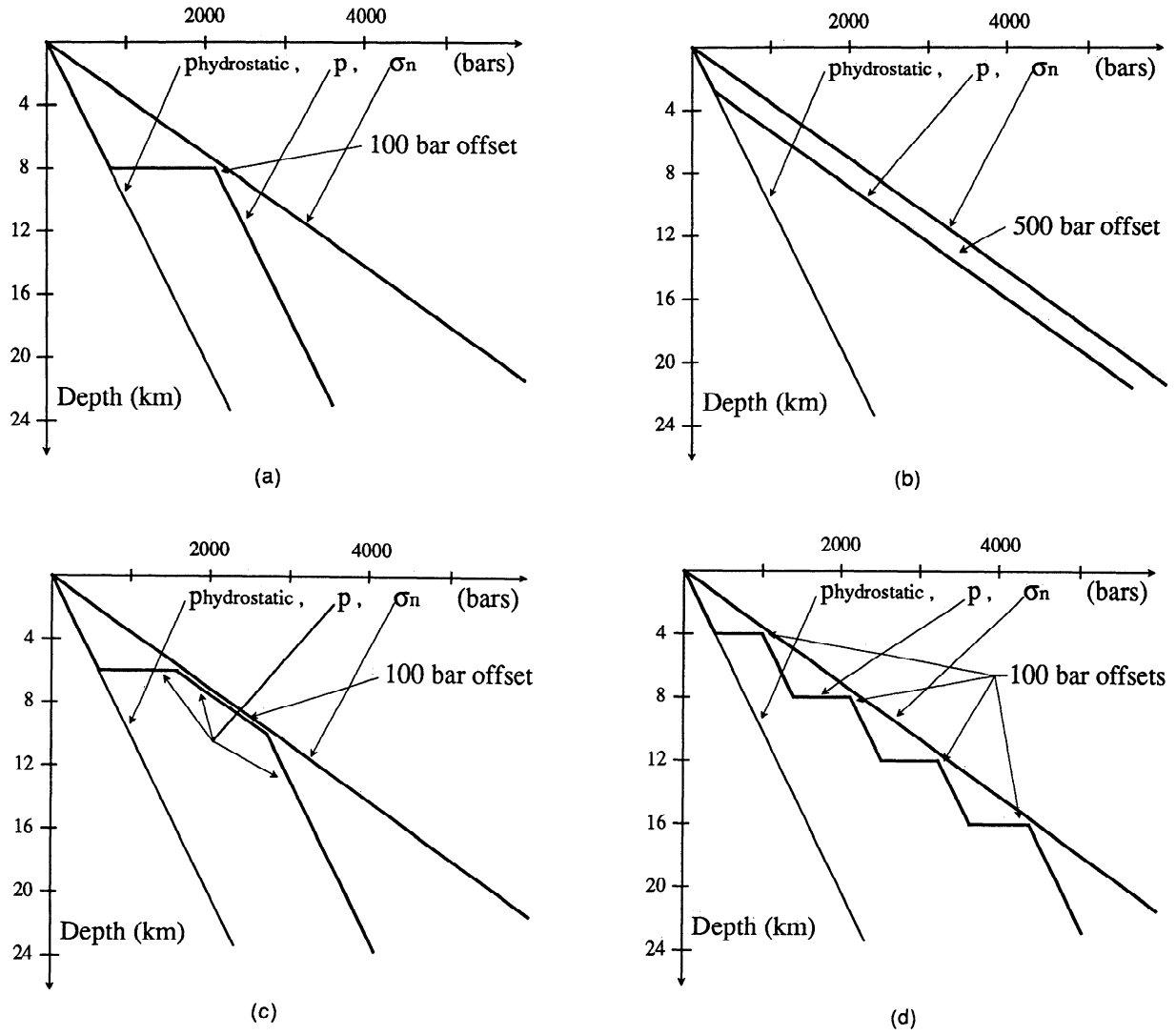

Figure 11. Pore pressure distributions used in calculations (cases I to VI) leading to Figures 12 and 13. Thin lines show hydrostatic pore pressure p; this pressure is used in for case I (Figure 12a). (a) Step to 10 MPa offset from lithostatic pressure σ_n at 8 km; case II (Figure 12b). (b) Lithostatic gradient with 50 MPa offset at depth; case III (Figure 12c) and case VI (Figure 13). (c) Step at 6 km with lithostatic gradient to 10 km and 10 MPa offset from σ_n; case IV (Figure 12d). (d) Four steps, each to 10 MPa offset from σ_n, at 4, 8, 12, and 16 km; case V (Figure 12e).

10 MPa below σ_n. This case represents a narrow but very low permeability layer that caps a deep high-p zone below 8 km. The resulting slip history is shown in Figure 12b, and, quite remarkably, even this very strong heterogeneity in p is insufficient to stop ruptures and generate a complex sequence of events. Slips are again shown every 5 years but now over a shorter total slip range of 6125 mm corresponding to 175 years of model evolution at 35 mm/yr. Since the pore pressure in this case is generally higher than in the previous example, the recurrence interval is shortened to 65 years.

Case III involves the pore pressure distribution of Figure 11b. Here the gradient begins as hydrostatic but changes to lithostatic [dp/d(depth) = $d\sigma_n/d$(depth)] such that p is offset by 50 MPa from σ_n beyond some shallow depth range. This type of distribution was considered by *Rice* [1993] as an example for a pore pressure with asymptotically lithostatic gradient, shown by *Rice* [1992] to result in a fault zone that is overpressurized at depth and has a permeability which decreases strongly with increasing $\sigma_n - p$. The slip history is shown in Figure 12c, where now there are 1-year intervals between the curves and the 3500-mm slip range corresponds to 100 years. Here the recurrence interval is further shortened, in accord with the generally higher p, to 41 yr.

Case IV corresponds to the p distribution of Figure 11c; after beginning with a hydrostatic gradient, p jumps at 6 km (e.g., a horizon of very low permeability), then continues between 6 and 10 km with a lithostatic gradient such that p is offset by only 10 MPa from σ_n, and finally continues with a hydrostatic gradient below 10 km. This pressure distribution is finally sufficient to induce some modest complexity in the earthquake history, as shown in Figure 12d; curves are again drawn every year and the slip range corresponds to 100 years. We now see that moderate events, rupturing below 6 km and inducing nearly coincident slip above 4 km, occur between

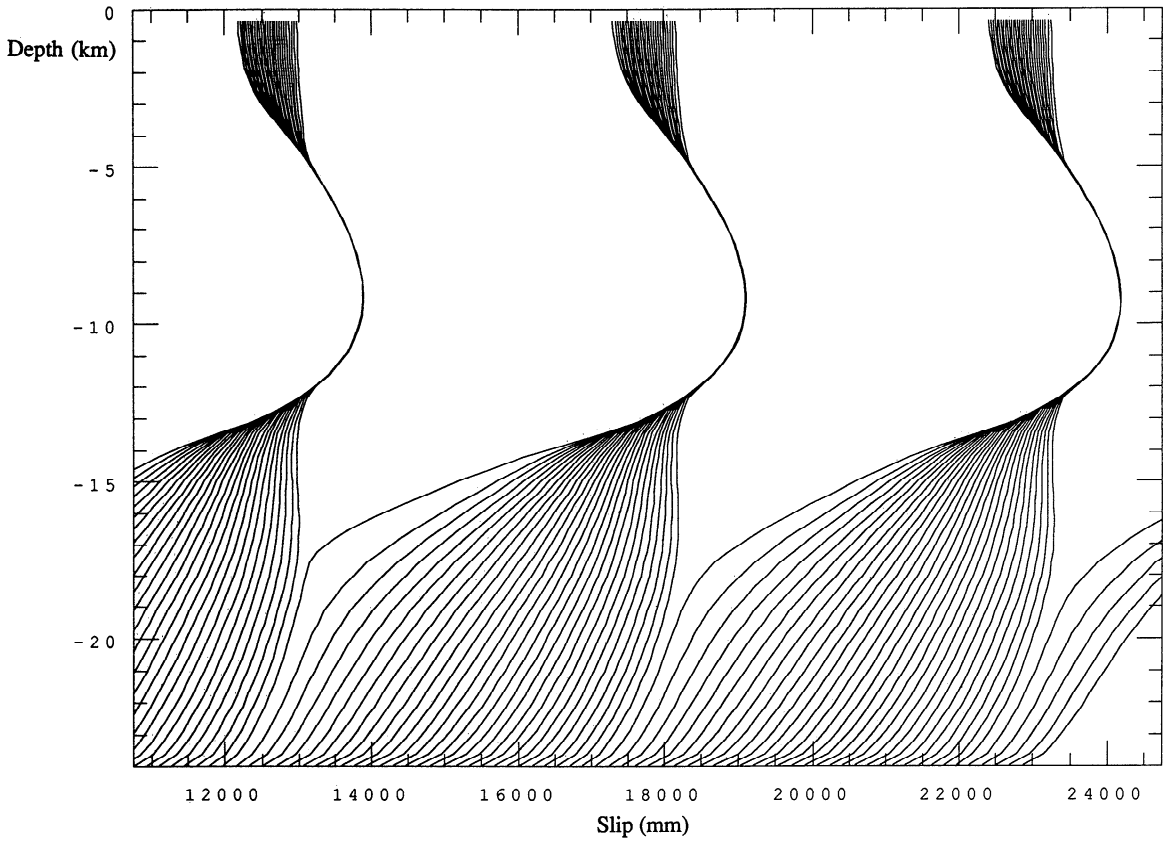

Figure 12a. Slip versus depth at 5-year intervals for case I; hydrostatic pore pressure.

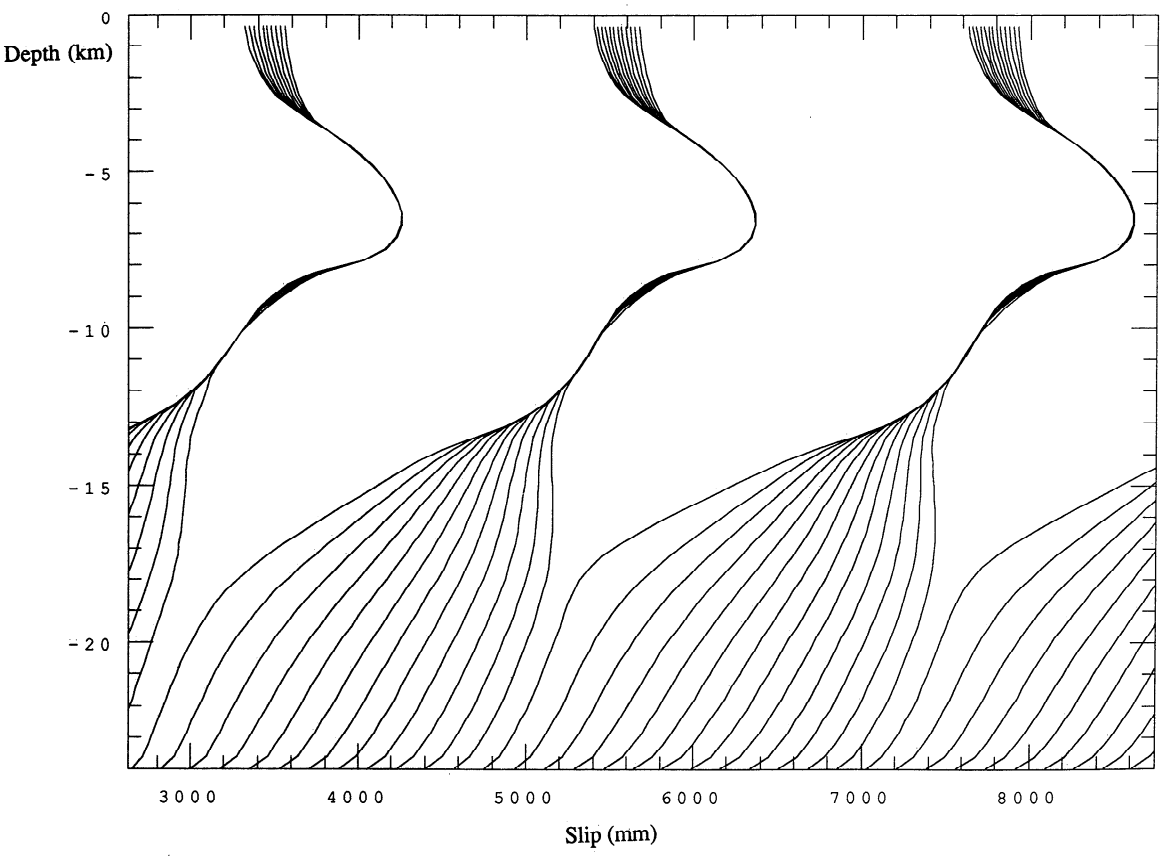

Figure 12b. Slip versus depth at 5-year intervals for case II; step in p to 10 MPa offset from σ_n at 8 km (Figure 11a).

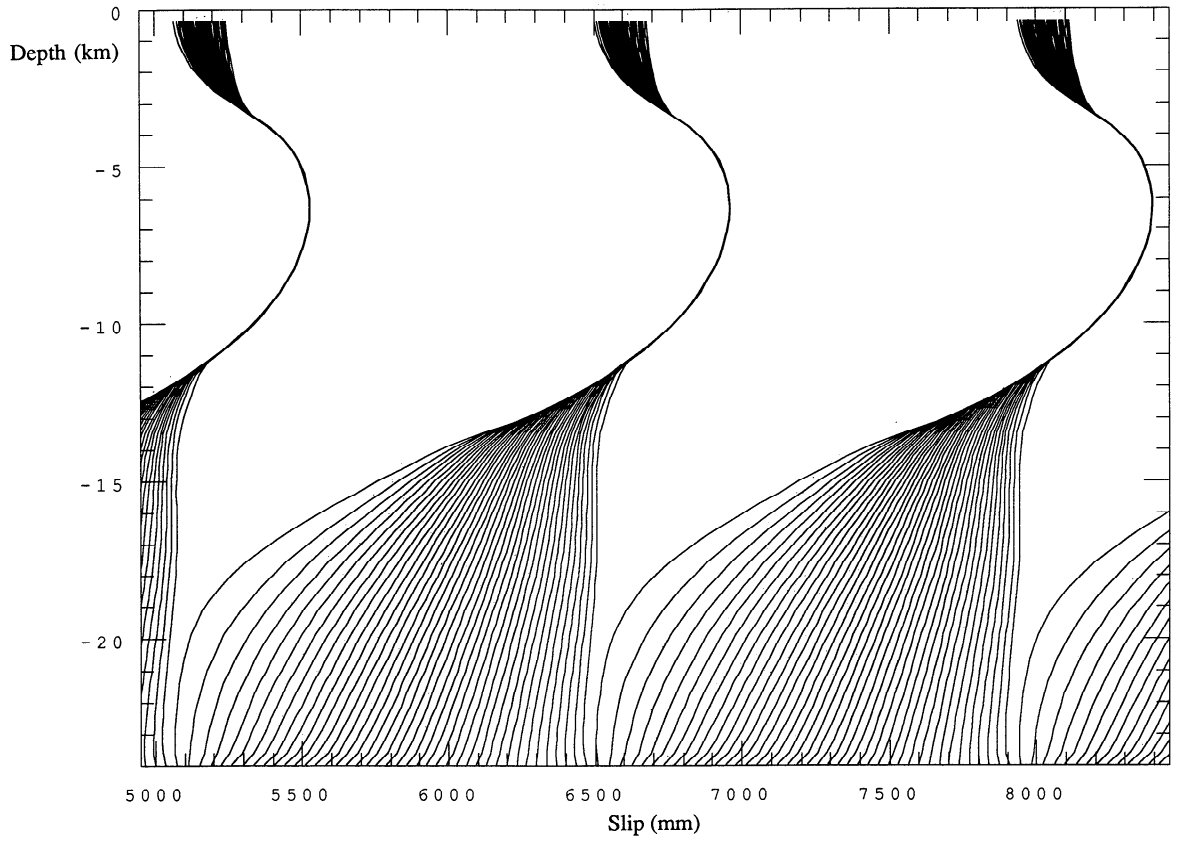

Figure 12c. Slip versus depth at 1-year intervals for case III; p has lithostatic gradient at depth and is offset 50 MPa from σ_n (Figure 11b).

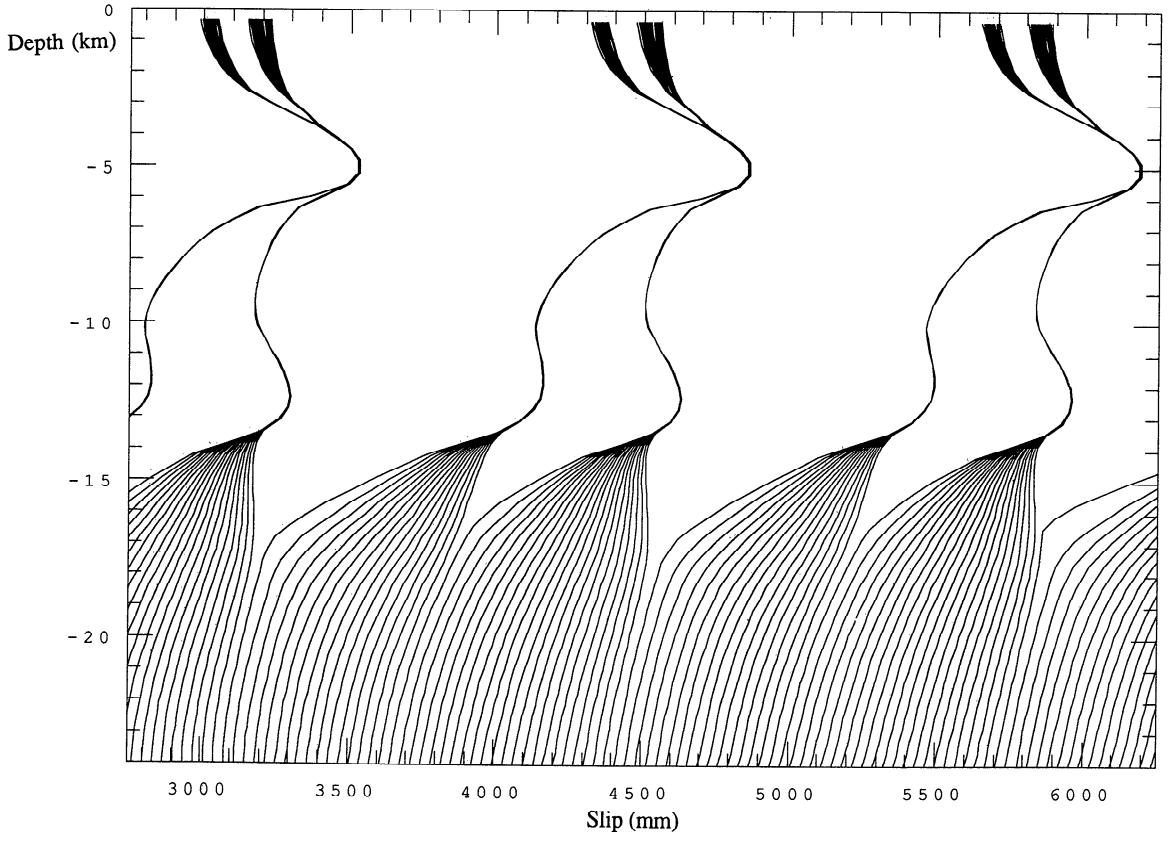

Figure 12d. Slip versus depth at 1-year intervals for case IV; p has step to 10 MPa offset from σ_n at 6 km and lithostatic gradient to 10 km (Figure 11c).

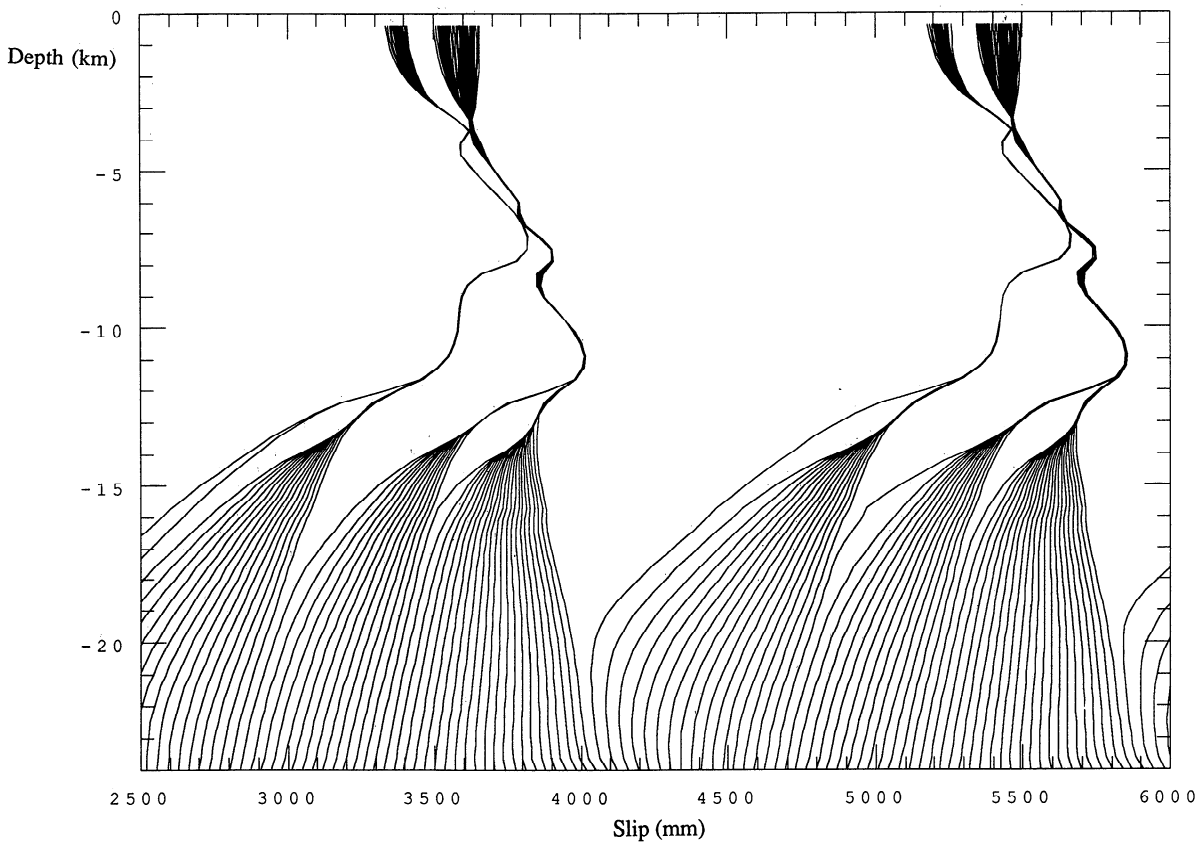

Figure 12e. Slip versus depth at 1-year intervals for case V; four steps of p, each to 10 MPa offset from σ_n, at 4, 8, 12 and 16 km (Figure 11d).

larger events that rupture the entire brittle crust. The recurrence interval for the large events is 38 years, and the moderate events occur 16 years into the large event cycle.

Case V corresponds to the four-step p distribution of Figure 11d. This might be thought of as a discontinuous version of the distribution in Figure 11b, in which permeable fault compartments, each 4 km deep and with hydrostatic gradient, are separated by very low permeability horizons at 4, 8, 12 and 16 km; each step raises p to 10 MPa below σ_n. The slip history is shown in Figure 12e, once again with 1-year intervals and slip range equivalent to 100 years. Now a complex sequence of earthquakes occurs. The large events have a 52-year recurrence interval, but around 1 year into their cycle the compartment between 12 and 16 km ruptures as a large aftershock. Then, 17 years into their cycle, a complex rupture occurs causing slip, or rapid afterslip, in all four compartments but with nodes at the bottom of the most shallow compartment and, surprisingly, 3/4 of the way down in the compartment below. At 30 years, the compartment between 12 and 16 km ruptures again. This case shows how strong heterogeneities of p, distributed over a fault zone, can induce complexities of rupture, although the matter is not very simple since the much stronger pressure step in Figure 11a (case II) was insufficient to induce complexity. One viable (but still unproved) working hypothesis is that the expedient of using oversized cells, or setting $L = 0$ like in the static/kinetic analysis discussed earlier, may represent the type of heterogeneity effects modeled in case V and other heterogeneities (presently too difficult to analyze) involving strong geometric disorder in the fault zone.

Figure 13 shows results for case VI, describing a fault model with strongly oversized cells. The calculations are based on the p distribution of Figure 11b, but general characteristics of the response with oversized cells do not seem strongly sensitive to details of the p distribution (e.g., the distribution of Figure 11d leads to roughly similar response), in contrast to the calculations which capture the continuum limit. Figure 13a shows the slip distributions at 5-year intervals; the range of the slip axis corresponds to 300 years at 35 mm/yr. Figure 13b shows distributions at 1-year intervals for a range of the slip axis corresponding to 110 years. This case involves an inherently discrete model and, consequently, the results are very different from those of cases I to V. Figures 13a and 13b show features like the cellular model discussed earlier with static/kinetic friction and $L = 0$. We note again that the results of Figure 12e, for the strongly heterogeneous but continuum model of case V, suggest a way in which the two classes of models might be reconciled.

For the small L values used in the calculations leading to Figures 12 and 13, essentially all slip over the velocity weakening range occurs as rupture instabilities. Figure 14 shows the average slip over 4 to 13 km depth as a function of time for case VI (oversized cells); the results are qualitatively similar to those shown in Figure 4 for the cellular static/kinetic friction model. The large model earthquakes are quasi-periodic, but the character of the events is variable. Modest bursts in seismicity occur sometimes but not always before the large ruptures, and not every burst in seismicity is followed by a large event. Figures 13a, 13b, and 12e suggest that a brittle zone at the border of an aseismically slipping

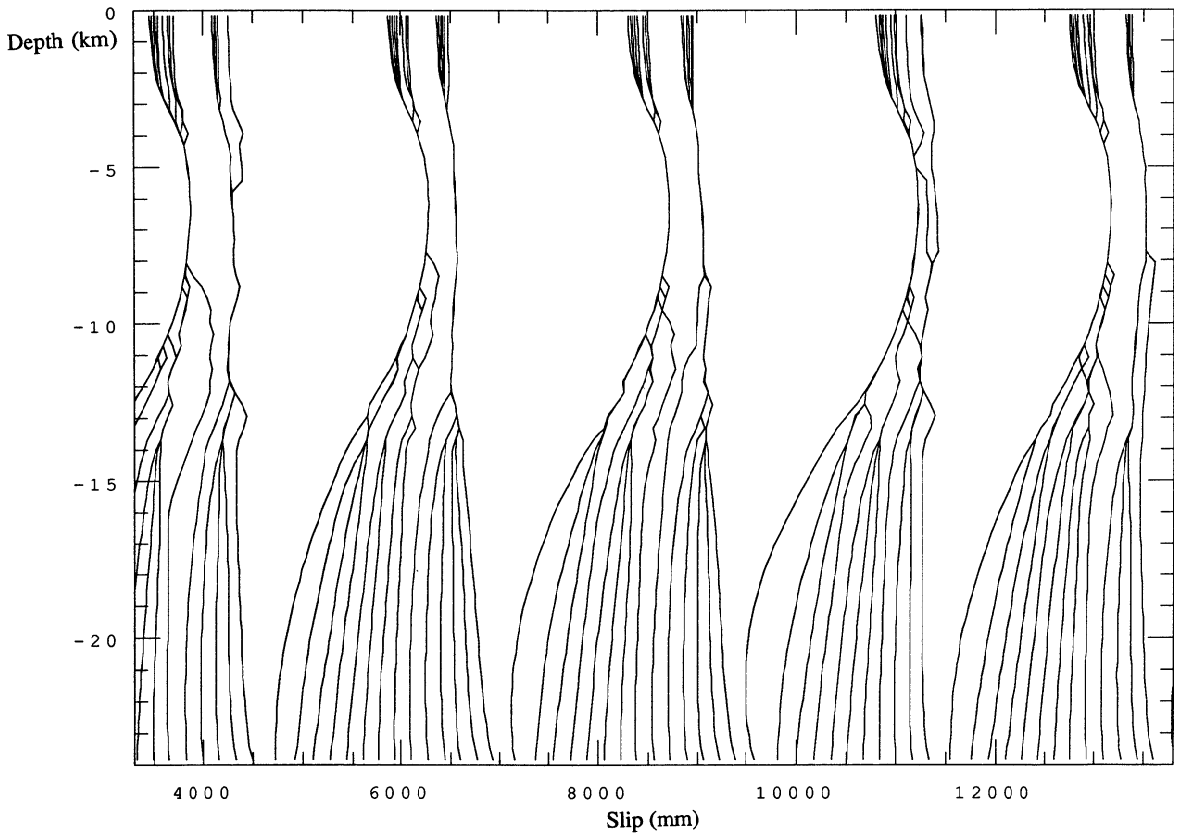

Figure 13a. Slip versus depth at 5-year intervals for case VI; oversized cells ($h^* = h/4$ in velocity weakening region); p has lithostatic gradient at depth and is offset 50 MPa from σ_n (Figure 11b).

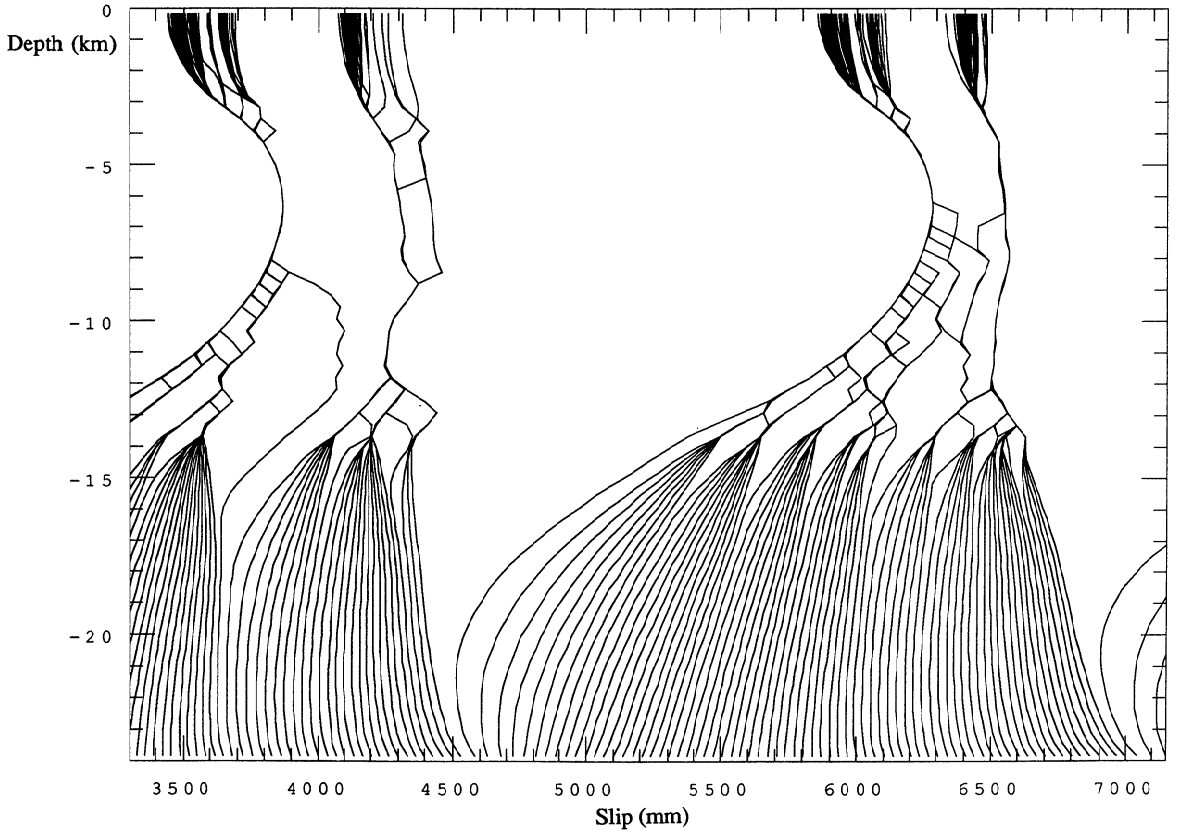

Figure 13b. Same as Figure 13a at 1-year intervals.

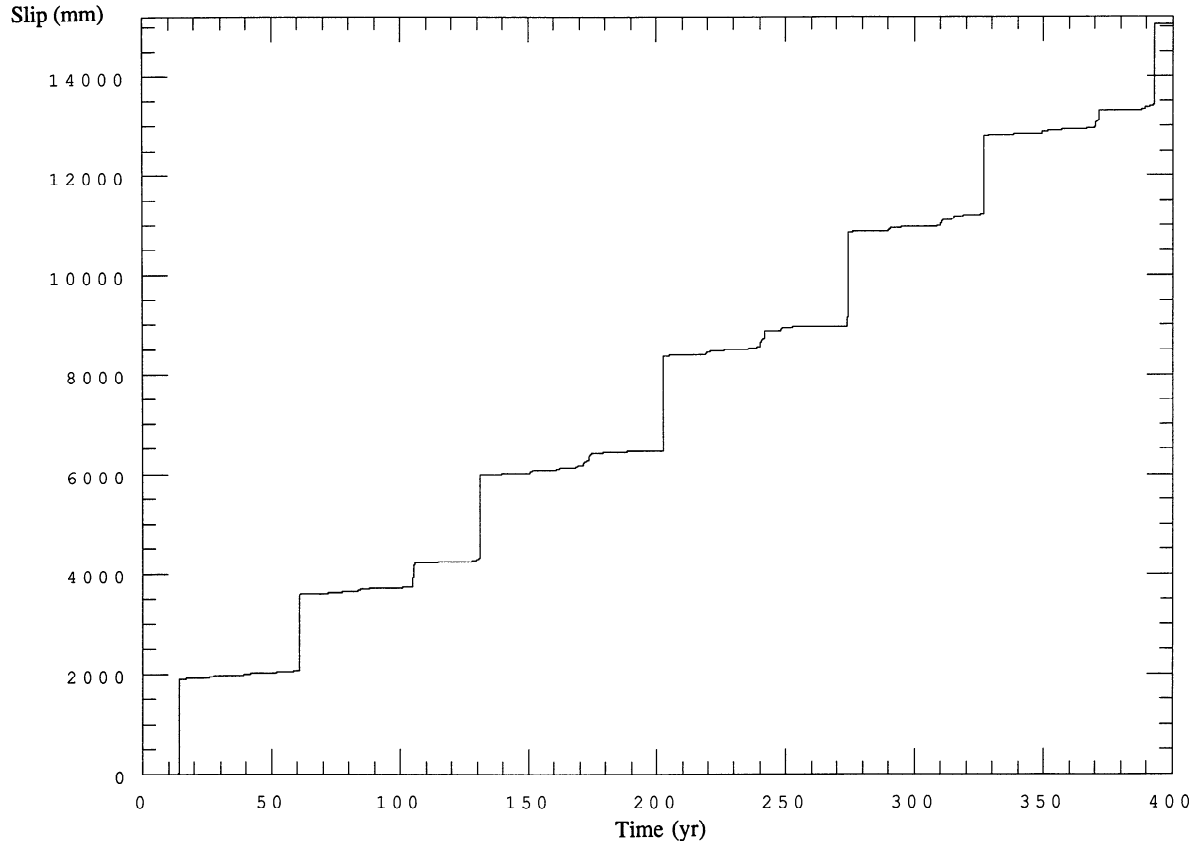

Figure 14. Average slip over the depth range 4-13 km versus time for case VI.

region can be a candidate for sequences of repeated small similar seismic events. The absence of small events in Figures 12a to 12d emphasizes the necessity for strong heterogeneity, adequate to stop seismic ruptures, for the occurrence of such sequences.

We now discuss results when, in place of (1), the Dieterich-Ruina "slowness" law is used. That law retains the first of equations (1), for f, but replaces ψ by $\ln (V_{pl}\,\theta/L)$ and rewrites the evolution law of state variable, i.e., the second of equations (1), as

$$d\theta/dt = 1 - \theta\,(d\delta/dt)/L\,. \qquad (3)$$

This is a true "ageing" law, in that here the state variable, and hence fault strength, continues to evolve even in the absence of slip, whereas the Ruina-Dieterich "slip" law (1) requires continuing slip for state evolution.

Numerical calculations were performed, with slip constrained as before to vary just with depth, $\delta = \delta(z, t)$, using the Dieterich-Ruina "slowness" law (3) for all the pore pressure distributions of cases I to V. The results are found to be generally similar to those obtained earlier. Extreme pore pressure variations are required to induce complexity into the simulated event sequences. As expected, the large earthquake recurrence times tend to lengthen. In addition, we do not always obtain periodic solutions; for example, case III (Figure 11b) leads to an apparently chaotic sequence of large events.

A more significant difference between predictions of the two friction laws was recently found in 3-D solutions, with slip $\delta = \delta\,(x, z, t)$, for the configuration of Figure 10 [*Rice*, 1994]. In these calculations, the modeled region consists of a given distance along strike (taken variously as 240, 480, or 960 km) with the slip pattern repeating periodically in x over that distance. The study was done for a pore pressure distribution like in Figure 11b but with a 100 MPa offset of p from σ_n at depth. The assumed distribution of a and b with depth was similar to that used before but with ±5-10% variations in different segments along strike to induce possible complex response.

In all 3-D cases considered, simulations based on the Ruina-Dieterich law (1) show a sequence of large, nearly identical ruptures which span the entire distance modeled along strike and repeat in a nearly periodic manner. Such is consistent with the results of *Rice* [1993], who used the same law. In contrast, simulations based on the Dieterich-Ruina law (3) show highly variable rupture lengths that rarely or never span the entire region modeled, and the history of events at any given location along strike is strongly aperiodic. On the other hand, events with length along-strike shorter than about 20 to 25 km, and with depth extent less than the 15 km depth range of the "brittle" crust, are never observed in the modeling. In agreement with our previous discussion, some representation of geometric disorder of fault zones at smaller scales is presumably necessary to explain smaller events. One may not, however, conclude that law (1) can never give complex slip in a continuum fault model; *Horowitz and Ruina* [1989] found complex response using that law, albeit with an added viscous term that prevented large variation in slip velocity.

Discussion

Variations of fluid pressure in fault zone rocks have long been recognized as being important for fault dynamics [e.g., *Nur*, 1972; *Sibson et al.*, 1975; *Rice*, 1979; *Rudnicki*, 1986].

Recent field, laboratory, and theoretical works [e.g., *Byerlee*, 1990, 1993; *Blanpied et al.*, 1992; *Sleep and Blanpied*, 1992; *Sibson*, 1992; *Rice*, 1992] generated renewed interest in the effects of fluid pressure on frictional properties of faults. In this paper we simulate fault instabilities in models emphasizing the dependency of fault friction on complex spatial distributions of geometrical irregularities, material heterogeneities, and pore pressure variations. The simulations are done using two separate categories of models. The first category, taken as an approximate representation of strong fault heterogeneity due to geometric disorder or other abrupt property variations, involves inherently discrete systems. This is modeled using both a cellular fault governed by static/kinetic friction [*Ben-Zion and Rice*, 1993], and a fault obeying rate- and state-dependent friction [*Rice*, 1993] but having numerical cells that are larger than a nucleation size for slip instabilities. The second category involves a continuum system representing a smooth fault surface subjected to various degrees of pore pressure variations. This is modeled by a fault satisfying rate- and state-dependent constitutive law, using numerical cells much smaller than the critical nucleation size. In both categories of models, stress transfers due to slip episodes are governed by 3-D continuum elasticity.

The results indicate that gradual pore pressure variations cannot explain the observed spatio-temporal complexity of seismic slip. It is possible, however, that the formation of seals [*Byerlee*, 1993] and localized zones that compact toward lithostatic p [*Sleep and Blanpied*, 1992; *Sleep*, this issue] could create strong and abrupt pore pressure fluctuations (e.g., of the type shown in Figures 2c and 11d) leading to complex seismic response. The simulations show that strong fault heterogeneity of the form envisioned in our models with discrete (quasi-independent) numerical cells is required for the generation of slip complexities, rough rupture fronts capable of radiating high-frequency seismic waves, and FS statistics of earthquakes having a wide range of event sizes. The large earthquakes simulated by the models are quasi-periodic; however, the character of the large events varies greatly from one sequence to the next. The results suggest that expectations for regular repeating sequences of earthquakes are unrealistic. This is supported by recent inversions of geodetic data along the central SAF, indicating that the 1934 and 1966 Parkfield earthquakes had substantially different rupture histories and/or distributions of slip [*Segall and Du*, 1993].

In the present work we are interested in the seismic response of a fault system over a time scale of hundreds to thousands of years. We assume that the first order mechanical properties of a fault system do not change much, in a statistical sense, over such periods. The above statement is equivalent to associating the first order mechanical properties of a fault system with first order structural features (fault bends, forks, stepovers) created by many earthquakes over many thousands of years. Fault properties are, of course, constantly evolving with time due to processes such as fresh fracture formation near geometrical incompatibilities [*King*, 1983; *Andrews*, 1989], gouge compaction [*Sleep and Blanpied*, 1992; *Sleep*, this issue], permeability reduction [*Moore et al.*, 1994], seismic fluid pumping [*Sibson*, 1992], pressure solution [*Hickman and Evans*, 1992], and a variety of other fluid-assisted mechanical and chemical processes described in this special section. In the current paper, however, we assume that the effect of such time-dependent processes on the strength of faults is, on the average, secondary to that of major structural discontinuities reflecting the overall deformational history of a fault. We thus keep the geometries, frictional properties, and tectonic loadings of the models constant in time. The time invariance of the above parameters leads to the existence of basic seismic cycles, manifested in quasi-periodicity of large events. On the other hand, the large number of quasi-independent fault segments (discrete numerical cells) and nonlinearities in the assumed friction laws produce variabilities in the timing and character of the large events. Thus our models generate quasi-periodic random sequences which may be viewed as resulting from a compromise between tendencies toward seismic cycle and predictability and tendencies toward randomness and chaos. This is illustrated in Figure 3 and Table 1, where the simulated results show a transition between fault behavior dominated by ingredients leading to periodicity, and seismic response dominated by ingredients leading to chaotic occurrence.

The frequency-size distribution of earthquakes is an important topic for both theoretical studies of earthquake dynamics and practical considerations of seismic hazard assessments. It is controversial whether FS statistics follow, in principle, a power law Gutenberg-Richter distribution, implying self-similarity over a broad range of earthquake magnitude, or whether earthquake statistics are characterized, intrinsically, by systematic strong deviations from self-similarity. The FS statistics of earthquakes observed along given faults or in seismogenic zones with uniform width and one (dominant) mode of faulting show in many cases [e.g., *Singh et al.*, 1983; *Schwartz and Coppersmith*, 1984; *Main and Burton*, 1984, 1989; *Davison and Scholz*, 1985; *Main*, 1987; *Trifu and Radulian*, 1991; *Wesnousky*, 1994] strong deviations from self-similarity and local maxima in the rate of events having "characteristic" rupture dimensions. On the other hand, the FS statistics of observed earthquakes "sampling" irregular seismogenic zones such as southern California [*Hileman et al.*, 1973] or the entire Earth [*Pacheco et al.*, 1992; *Kagan*, 1993, 1994] show a broad power law distribution. The observations suggest the existence of a "fundamental" FS distribution of earthquakes with features (and information) not accounted for by the simple GR relation, and that the latter broad power law GR statistics result from a secondary "averaging" process. This hypothesis is supported by the analysis of *Ben-Zion and Rice* [1993] and the present work.

Our results indicate that in a system characterized by geometric disorder (i.e., strength heterogeneity) spanning a narrow range of size scales, with stress transfer governed by 3-D continuum elasticity, the FS statistics of earthquakes can be self-similar only over a narrow range of events smaller than a critical size. This is due to the fact that the stress concentrated in a 3-D elastic solid at the edge of an expanding rupture grows with the rupture size. Thus, when the fault is characterized by a narrow range of geometric disorder, as in cases 1-4 of the analysis, the scaling of stress concentrations with the rupture size introduces a critical event size terminating the range of self-similar earthquake statistics. In such systems, events reaching the critical size become (on the average) unstoppable, and they continue to grow to a size limited by a characteristic system dimension (see Figures 7 and 8). When, however, the system is characterized by a broad spectrum of geometric disorder, as in case 5 of the analysis, a corresponding broad spectrum of critical event sizes exists,

and the phenomena discussed above are suppressed (Figure 9). The simulations indicate that rupture areas terminating the self-similar range of FS statistics are related to dominant length scales characterizing the system heterogeneities, and that local maxima in FS statistics correspond to dimensions of coherent brittle zones such as the width of the seismogenic layer or the length of a fault segment bounded by barriers. Thus observed FS statistics can be used to derive information on crustal thickness and fault zone structure. Our analysis offers a coherent explanation for both the GR statistics and the characteristic earthquake distribution of seismicity. The results suggest that the frequency of occurrence of moderate and strong earthquakes is enhanced with respect to self-similar distributions defined by small events, whether local maxima are observed in the FS statistics or are averaged out.

The notion that earthquakes are dynamically self-similar is very attractive on grounds of simplicity and analogy to other natural systems. However, the observations and analysis mentioned above indicate that continuum elasticity, coupled with a given segmented (discrete) fault zone structure, can produce a length scale (event diameter about $16h$ in our simulations [*Ben-Zion and Rice*, 1993, Table 1]) terminating the self-similar regime of earthquake dynamics. The range of the self-similar regime can be extended by the existence of barriers that can stop ruptures at yet larger scales (see, e.g., Figures 2c and 9). As discussed by *Ben-Zion and Rice* [1993], a lower length scale that may limit self-similarity of earthquakes is the width of fault zones. This size scale is a natural unit for measuring structural fault zone discontinuities, and it may thus provide a basis for choosing h when using the inherently discrete fault models. Analytic waveform fits of seismic fault zone trapped and head waves [*Leary and Ben-Zion*, 1992; *Ben-Zion*, 1993; *Hough et al.*, 1994] indicate that the width of mature fault zones is of the order of a few hundreds of meters. Numerous seismological observations for small earthquakes, including the constancy of their radiated corner frequency [e.g., *Chouet et al.*, 1978; *Fletcher*, 1980], the strong variation of their stress drops [e.g., *Sacks and Rydelek*, 1992; *Hough et al.*, 1992], and their deviations from self-similar FS statistics [e.g., *Aki*, 1987; *Malin et al.*, 1989; *Rydelek and Sacks*, 1989; *Sacks and Rydelek*, 1992], may be related to the width of the corresponding fault zone and may hence also be used to estimate the size of h (we note that these observations may also result from site and recording effects; see related discussion and references of *Ben-Zion and Rice* [1993]). A third length scale that is an obvious candidate for disrupting self-similar seismic response is the width of the brittle seismogenic zone (about 10-15 km for the SAF; 30-100 km for subduction zones). *Pacheco et al.* [1992], using least squares analysis, claimed to have identified a break in the slope (power) of observed FS statistics of global earthquakes related to an average size of the seismogenic zone. However, *Kagan* [1993, 1994], using the presumably superior maximum likelihood procedure, found that FS distribution of global earthquakes in the high-quality Harvard catalog does not show a break of slope corresponding to the seismogenic layer.

Our analysis indicates that the range of size scales characterizing fault zone properties has various manifestations in the seismic response of a fault. The significant enhancement in the rate of occurrence of the $M \approx 6$ Parkfield earthquakes with respect to power law extrapolation of the low-magnitude background seismicity [*Ben-Zion and Rice*, 1993, Figure 15], and the ratio mean/standard-deviation (≈ 3) of the time intervals separating the $M \approx 6$ Parkfield events (as well as the corresponding ratio of calculated time-dependent slip deficits between the events) [*Ben-Zion et al.*, 1993, Table 2] suggest that the structure of the San Andreas fault at Parkfield is characterized by a narrow range of size scales. This is compatible with high-resolution borehole seismic observations of *Johnson and McEvilly* [this issue], showing that the spatial distribution of Parkfield seismicity (over the 1987-1993 period of high-resolution borehole measurements) exhibits a fairly regular pattern consisting of alternating regions, 3-6 km in dimension, of high and low seismic activity. These regions of alternating seismic activity may reflect structurally dominated hydrological fault zone compartments. Fault-trace-complexity analyses of *Wesnousky* [1988, 1994] indicate that the geometry of fault zone structures becomes progressively more regular with cumulative slip. Since the central SAF experienced a cumulative slip of a few hundreds of kilometers, the fault-trace-complexity data of Wesnousky provide an additional support for our suggestion, based on statistics of earthquakes, that the SAF at Parkfield is characterized by a narrow range of size scales. A process competing with the smoothing of geometrical fault zone irregularities with cumulative slip [*Wesnousky*, 1988] is that of "block rotations," making a fault system progressively missaligned with respect to the far-field plate motion with age or cumulative slip [e.g., *Freund*, 1974; *Ron et al.*, 1984; *Nur et al.*, 1993]. Thus there can be transition times (e.g., the recent period for the central-Mojave/eastern-California-shear-zone [*Nur et al.*, 1993]) during which old geometrically ordered but unfavorably aligned faults become deactivated, new geometrically disordered, favorably aligned fault systems are formed (e.g., the rupture zone of the 1992 Landers, California, earthquake), and a new evolution cycle of fault zone structure begins.

It is worthwhile to close the discussion by mentioning a few shortcomings of our work. The simulations of *Ben-Zion and Rice* [1993] and the first section of our analysis model all slip episodes as brittle failures. This ignores time-dependent effects due to viscoelasticity in the lower crust [e.g., *Li and Rice*, 1987; *Ben-Zion et al.*, 1993], and aseismic slip in creeping fault sections and in small slip patches within the computational grid [e.g., *Dieterich*, 1986; *Tse and Rice*, 1986; *Rice*, 1993]. As shown by *Ben-Zion et al.* [1993], however, slip velocities in the lower crust, and hence loading rates on the upper seismogenic layer, are expected to vary in time throughout an entire great earthquake cycle. Shortly after an 1857-type earthquake slip rates in the viscoelastic lower crust are higher than the far-field plate velocity, while later in the cycle they are lower. High loading rates early in the cycle may result in clustering of earthquakes in space and time, while low loading rates late in the cycle may result in an overall decrease of activity. Similarly, time-varying stress concentrations due to aseismic slip in small slip patches (i.e., patches with size $h < h^*$) and in creeping fault sections can have important effects on foreshock-mainshock-aftershock sequences. The modeling of these time-dependent effects can be achieved by incorporating features of rate- and state-dependent friction and/or creep law into the constitutive stress-slip relation.

The simulations of *Rice* [1993], *Ben-Zion and Rice* [1993], and the present work model inertial effects during seismic slip only approximately (e.g., by a seismic radiation damping term for rapid slip along the fault, or by allowance for dynamic overshoot in rupture arrest). Thus calculated final states of stress on the fault after failures can be correct only in an approximate sense. It is important to examine whether a more

precise treatment of elastodynamics during instabilities would qualitatively modify critical features of the modeling results, in a way that would change our conclusions on features responsible for slip complexity. As suggested by, e.g., *Cochard and Madariaga* [1994], *Shaw* [1994], and *Madariaga and Cochard* [1994], it is perhaps possible that the wave-mediated arrest of a dynamic slip event will leave a heterogeneous distribution of residual static stress on the ruptured surface. Such heterogeneity, if strong enough, could affect the nucleation and arrest locations of subsequent ruptures and may become a mechanism for sustaining complex seismic behavior. However, dynamic simulations [*Andrews*, 1975; *Rice and Ben-Zion*, submitted manuscript, 1995; *Y. Ben-Zion et al.*, manuscript in preparation, 1995] in uniform models without strong implicit heterogeneities (due to, e.g., inherent model discreteness and/or highly heterogeneous initial and boundary conditions), and with proper calculations of stress concentrations, have not generated realistic complex slip sequences for parameter ranges examined so far, and they thus contradict the hypothesis that seismic complexities are a generic outcome of inertial dynamics. On the other hand, recent analysis of a dynamic crack growing spontaneously over a plane in a 3-D elastic solid [*Rice et al.*, 1994; *Perrin and Rice*, 1994] indicate that dynamic processes may interact strongly with a small amount of heterogeneity, leading to large spatial and temporal fluctuations in crack front velocities and positions. As another example, seismic *P* head waves propagating along fault zone material interfaces [e.g., *Ben-Zion*, 1990; *Ben-Zion and Malin*, 1991; *Hough et al.*, 1994] can create an oscillatory normal stress regime, modulating dynamically the (possibly homogeneous) frictional properties of a fault. (Other mechanisms for normal stress variations, some involving material contrast across a fault, e.g., *Schallamach* [1971], are discussed by *Brune et al.* [1993].) Finally, the large off-fault stresses generated near a rupture front as it accelerates toward its limiting speed [e.g., *Rice*, 1980] could promote non planar rupture features and be a further factor inducing complex response.

Our results indicate that strong fault heterogeneities, probably due to geometric disorder and possibly also extreme pore pressure fluctuations, are responsible for the complexity of observed fault behavior. We have used planar cellular fault zone models to simulate different types of strong heterogeneities, assuming that a 3-D network of geometrical fault zone disorder can be mapped onto a 2-D plane. It is important to rationalize such a mapping in future work.

Acknowledgments. We thank Joe Andrews, Yan Kagan, Leon Knopoff, and Raul Madariaga for discussions and Steve Brown for a program generating fractal surfaces. The manuscript benefited from comments by Joe Andrews, Steve Day, Mariana Eneva, Steve Hickman, and Sue Hough. The work was supported by the Southern California Earthquake Center (subcontract 569928 from USC, based on NSF support), and the USGS National Earthquake Hazard Reduction Program (grant 1434-93-G-2276). A preliminary version of the paper [*Ben-Zion and Rice*, 1994] has been presented in a USGS Conference Proceedings.

References

Aki, K., Magnitude-frequency relation for small earthquakes: A clue to the origin of f_{max} of large earthquakes, *J. Geophys. Res.*, *92*, 1349-1355, 1987.

Andrews, D. J., From antimoment to moment: plane-strain models of earthquakes that stop, *Bull. Seismol. Soc. Am.*, *65*, 163-182, 1975.

Andrews, D. J., A stochastic fault model, 1, Static case, J. *Geophys. Res.*, *85*, 3867-3877, 1980.

Andrews, D. J., A stochastic fault model, 2, Time-dependent case, *J. Geophys. Res.*, *86*, 10,821-10,834, 1981.

Andrews, D. J., Dynamic plane-strain shear rupture with a slip-weakening friction law calculated by a boundary integral method, *Bull. Seismol. Soc. Am.*, *75*, 1-21, 1985.

Andrews, D. J., Mechanics of fault junctions, *J. Geophys. Res.*, *94*, 9389-9397, 1989.

Aviles, C. A., C. H. Scholz, and J. Boatwright, Fractal analysis applied to characteristic segments of the San Andreas Fault, *J. Geophys. Res.*, *92*, 331-334, 1987.

Bak, P., and C. Tang, Earthquakes as self-organized critical phenomena, *J. Geophys. Res.*, *94*, 15,635-15,637, 1989.

Ben-Zion, Y., The response of two half spaces to point dislocations at the material interface, *Geophys. J. Int.*, *101*, 507-528, 1990.

Ben-Zion, Y., Structure of a few fault segments in California from travel time inversion and waveform modeling of fault zone seismic waves, *Ann. Geophys.*, *11*, suppl. I, c47, 1993.

Ben-Zion, Y., and P. Malin. San Andreas fault zone head waves near Parkfield, California, *Science*, *251*, 1592-1594, 1991.

Ben-Zion, Y., and J. R. Rice, Earthquake failure sequences along a cellular fault zone in a three-dimensional elastic solid containing asperity and nonasperity regions, *J. Geophys. Res.*, *98*, 14,109-14,131, 1993.

Ben-Zion, Y., and J. R. Rice, Quasi-static simulations of earthquakes and slip complexity along a 2D fault in a 3D elastic solid, in The Mechanical Involvement of Fluids in Faulting, *U. S. Geol. Surv. Open File Rep., 94-228*, 406-435, 1994.

Ben-Zion, Y., J. R. Rice, and R. Dmowska, Interaction of the San Andreas fault creeping segment with adjacent great rupture zones and earthquake recurrence at Parkfield, *J. Geophys. Res.*, *98*, 2135-2144, 1993.

Blanpied, M. L., D. A. Lockner, and J. D. Byerlee, Fault stability inferred from granite sliding experiments at hydrothermal conditions, *Geophys. Res. Lett.*, *18*(4), 609-612, 1991.

Blanpied, M. L., D. A. Lockner, and J. D. Byerlee, An earthquake mechanism based on rapid sealing of faults, *Nature*, *358*, 574-358, 1992.

Brown, S. R. , Simple mathematical models of a rough fracture, manuscript, *J. Geophys. Res.*, in press, 1995.

Brune, J. N., S. Brown, and P. A. Johnson, Rupture mechanism and interface separation in foam rubber model of earthquakes: A possible solution to the heat flow paradox and the paradox of large overthrusts, *Tectonophysics*, *218*, 59-67, 1993.

Burridge, R., and L. Knopoff, Model and theoretical seismicity, *Bull. Seismol. Soc. Am.*, *57*, 341-371, 1967.

Byerlee, J. D. Friction, overpressure and fault normal compression, *Geophys. Res. Lett.*, *17*, 2109-2112, 1990.

Byerlee, J. Model for episodic flow of high-pressure water in fault zones before earthquakes, *Geology*, *21*, 303-306, 1993.

Carlson, J. M., and J. S. Langer, Mechanical model of an earthquake, *Phys. Rev. A*, *40*, 6470-6484, 1989.

Carlson, J. M., J. S. Langer, B. Shaw, and C. Tang, Intrinsic properties of a Burridge-Knopoff model of a fault, *Phys. Rev. A*, *44*, 884-897, 1991.

Chinnery, M., The stress changes that accompany strike-slip faulting, *Bull. Seismol. Soc. Am.*, *53*, 921-932, 1963.

Chouet, B., K. Aki, and M. Tsujiura, Regional variation of the scaling law of earthquake source spectra, *Bull. Seismol. Soc. Am.*, *68*, 49-79, 1978.

Cochard, A., and R. Madariaga, Dynamic faulting under rate-dependent friction, *Pure Appl. Geophys.*, *142*, 419-445, 1994.

Davison, F. C., and C. H. Scholz, Frequency-moment distribution of earthquakes in the Aleutian arc: A test of the characteristic earthquake model, *Bull. Seismol. Soc. Am.*, *75*, 1349-1361, 1985.

Day, M. S., Three-dimensional simulation of spontaneous rupture: The

effect of nonuniform prestress, *Bull. Seismol. Soc. Am.*, *72*, 1889-1902, 1982.

Dieterich, J. H., A model for the nucleation of earthquake slip, in *Earthquake Source Mechanics, Geophys. Monogr. Ser.*, vol. 37, edited by S. Das, J. Boatwright, and C. H. Scholz, pp. 37-47, AGU, Washington, D. C., 1986.

Dieterich, J. H., Earthquake nucleation on faults with rate- and state-dependent strength, *Tectonophysics*, *211*, 115-134, 1992.

Fletcher, J. B., Spectra from high-dynamic range digital recording of Oroville, California, aftershocks and their source parameters, *Bull. Seismol. Soc. Am.*, *70*, 735-755, 1980.

Frankel, A., High-frequency spectral falloff of earthquakes, fractal dimension of complex rupture, *b* value, and the scaling of strength on faults, *J. Geophys. Res.*, *96*, 6291-6302, 1991.

Freund, R., Kinematics of transform and transcurrent faults, *Tectonophysics*, *21*, 93-134, 1974.

Gao, H., J. J. Rice, and J. Lee, Penetration of a quasi-statically slipping crack into a seismogenic zone of heterogeneous fracture resistance, *J. Geophys. Res.*, *96*, 21,535-21,548, 1991.

Hanks, T. C., and H. Kanamori, A moment magnitude scale, *J. Geophys. Res.*, *84*, 2348-2350, 1979.

Harris, R. A., and S. M. Day, Dynamics of fault interaction: Parallel strike-slip faults, *J. Geophys. Res.*, *98*, 4461-4472, 1993.

Harris, R. A., and P. Segall, Detection of a locked zone at depth on the Parkfield, California, segment of the San Andreas fault, *J. Geophys. Res.*, *92*, 7945-7962, 1987.

Hickman, S., and B. Evans, Growth of grain contacts in halite by solution transfer: Implications for diagenesis, lithfication, and strength recovery, in *Fault Mechanics and Transport Properties of Rocks*, pp. 253-280, Academic, San Diego, Calif., 1992.

Hileman, J. A., C. R. Allen, and J. M. Nordquist, Seismicity of the southern California region 1st Jan. 1932 to 31st Dec. 1972, *Contrib. N. 2385*, Div. of Geol. and Planet. Sci., Calif. Inst. of Technol., Pasadena, Calif., 1973.

Horowitz, F. G., and A. Ruina, Slip patterns in a spatially homogeneous fault model, *J. Geophys. Res.*, *94*, 10,279-10,298, 1989.

Hough, S. E., H. Gue, A. Lerner-Lam, S. Seeber, and C. Scholz, Stress drop scaling: Results from empirical Green's function study of Loma Prieta aftershocks, *Seismol. Res. Lett.*, *63*(1), 24, 1992.

Hough, S. E., Y. Ben-Zion, and P. Leary, Fault-zone waves observed at the southern Joshua Tree earthquake rupture zone, *Bull. Seismol. Soc. Am.*, *84*, 761-767, 1994.

Ito, K., and M. Matsuzaki, Earthquakes as self organized critical phenomena, *J. Geophys. Res.*, *95*, 6853-6860, 1990.

Johnson, P., and T. V. McEvilly, Parkfield seismicity: Fluid driven?, *J. Geophys. Res.*, this issue.

Kagan, Y. Y., Stochastic model of earthquake fault geometry, *Geophys. J. R. Astron. Soc.*, *71*, 659-691, 1982.

Kagan, Y. Y., Fractal dimension of brittle fracture, *J. Nonlinear Sci.*, *1*, 1-16, 1991.

Kagan, Y. Y., Statistics of characteristic earthquakes, *Bull. Seismol. Soc. Am.*, *83*, 7-24, 1993.

Kagan, Y. Y., Observational evidence for earthquakes as a nonlinear dynamic process, *Physica D*, *77*, 160-192, 1994.

Kagan Y. Y., and D. D. Jackson, Long-term earthquake clustering, *Geophy. J. Int.*, *104*, 117-133, 1991.

Kagan, Y. Y., and L. Knopoff, Stochastic synthesis of earthquake catalogs, *J. Geophys. Res.*, *86*, 2853-2862, 1981.

King, G. The accommodation of large strains in the upper lithosphere of the Earth and other solids by self-similar fault systems: The geometrical origin of b-value, *Pure Appl. Geophys.*, *121*, 761-814, 1983.

Kostrov, B. V., Unsteady propagation of longitudinal shear cracks, *J. Appl. Math. Mech.*, *30*, 1241-1248, 1966.

Leary P., Deep borehole log evidence for fractal distribution of fractures in crystalline rock, *Geophys. J. Int.*, *107*, 615-627, 1991.

Leary, P., and Y. Ben-Zion, A 200 m wide fault zone low velocity layer on the San Andreas fault at Parkfield: Results from analytic waveform fits to trapped wave groups, *Seismol. Res. Lett.*, *63*, 62, 1992.

Li, V. C., and J. R. Rice, Crustal deformation in great California earthquake cycles, *J. Geophys. Res.*, *92*, 11,533-11,551, 1987.

Lomnitz-Adler, J., Automaton models of seismic fracture: Constraints imposed by the magnitude-frequency relation, *J. Geophys. Res.*, *98*, 17,745-17,756, 1993.

Madariaga, R. and A. Cochard, The dynamic origin of earthquake complexity, *Eos Trans. AGU*, *75*(44), Fall Meeting suppl., 426-427, 1994.

Main, I. G., A characteristic earthquake model of the seismicity preceding the eruption of Mount St. Helens on 18 May 1980, *Phys. Earth Planet. Inter.*, *49*, 283-293, 1987.

Main, I. G., and P. W. Burton, Physical links between crustal deformation, seismic moment and seismic hazard for regions of varying seismicity, *Geophys. J. R. Astron. Soc.*, *79*, 469-488, 1984.

Main, I. G., and P. W. Burton, Seismotectonics and the earthquake frequency-magnitude distribution in the Aegean area, *Geophys. J.*, *98*, 575-586, 1989.

Malin, P. E., S. N. Blakeslee, M. G. Alvarez, and A. J. Martin, Microearthquake imaging of the Parkfield asperity, *Science*, *244*, 557-559, 1989.

Mikumo, T., and T. Miyatake, Numerical modelling of space and time variations of seismic activity before major earthquakes, *Geoph. J. R. Astr. Soc.*, *74*, 559-583, 1983.

Moore, D. E., D. A. Lockner, and J. D. Byerlee, Reduction of permeability in granite at elevated temperature, *Science*, *265*, 1558-1561, 1994.

Nadeau, R., M. Antolik, P. A. Johnson, W. Foxall, and T. E. McEvilly, Seismological studies at Parkfield, III, Microearthquake clusters in the study of fault-zone dynamics, *Bull. Seismol. Soc. Am.*, *84*, 247-263, 1994.

Nur, A., Dilatancy, pore fluids, and premonitory variations of t_s/t_p travel times, *Bull. Seismol. Soc. Am.*, *62*, 1217-1222, 1972.

Nur, A., H. Ron, and G. Beroza, The nature of the Landers-Mojave earthquake line, *Science*, *261*, 201-203, 1993.

Okubo, P. G., Dynamic rupture modeling with laboratory-derived constitutive relations, *J. Geophys. Res.*, *94*, 12,321-12,335, 1989.

Okubo, P., and K. Aki, Fractal geometry in the San Andreas fault system, *J. Geophys. Res.*, *92*, 345-355, 1987.

O'Neill, M. E., Source dimensions and stress drops of small earthquakes near Parkfield, California, *Bull. Seismol. Soc. Am.*, *74*, 27-40, 1984.

Pacheco, J. F., C. H. Scholz, and L. R. Sykes, Changes in frequency-size relationship from small to large earthquakes, *Nature*, *255*, 71-73, 1992.

Perrin, G. O., and J. R. Rice, Disordering of a dynamic planar crack front in a model elastic medium of randomly variable toughness, *J. Mech. Phys. Solids*, *42*, 1047-1064, 1994.

Power, W. L., and T. E. Tullis, Euclidian and fractal models for the description of rock surface roughness, *J. Geophys. Res.*, *96*, 415-424, 1991.

Power, W. L., T. E. Tullis, and J. D. Weeks, Roughness and wear during brittle faulting, *J. Geophys. Res.*, *93*, 15,268-15,287, 1988.

Rice, J. R., Theory of precursory processes in the inception of earthquake rupture, *Gerlands Beitr. Geophys.*, *88*, 91-127, 1979.

Rice, J. R., The mechanics of earthquake rupture, in *Physics of the Earth's Interior*, edited by A. M. Dziewonski, and E. Boschi, pp. 555-649, North-Holland, Amsterdam, 1980.

Rice, J. R., Fault stress states, pore pressure distributions, and the weakness of the San Andreas fault, in *Fault Mechanics and Transport Properties of Rocks*, pp. 475-503, Academic, San Diego, Calif., 1992.

Rice, J. R., Spatio-temporal complexity of slip on a fault, *J. Geophys. Res.*, *98*, 9885-9907, 1993.

Rice, J. R., Comparison of slip complexity produced by two rate- and state-dependent friction laws, *Eos Trans. AGU, 75*, 441, 1994.

Rice J. R., Y. Ben-Zion, and K. S. Kim, Three-dimensional perturbation solution for a dynamic planar crack moving unsteadily in a model elastic solid, *J. Mech. Phys. Solids, 42*, 813-843, 1994.

Ron, H., R. Freund, Z. Garfunkel, and A. Nur, Block rotation by strike-slip faulting: Structural and paleomagnetic evidence, *J. Geophys. Res., 89*, 6256-6270, 1984.

Rudnicki, J. W., Slip on an impermeable fault in a fluid-saturated rock mass, in *Earthquake Source Mechanics, Geophys. Monogr. Ser.*, vol. 37, edited by S. Das, J. Boatwright, and C. H. Scholz, pp. 81-89, AGU, Washington, D. C., 1986.

Rundle, J. B., A physical model for earthquakes, 1, Fluctuations and interactions, *J. Geophys. Res., 93*, 6237-6254, 1988.

Rydelek, P. A., and I. S. Sacks, Testing the completeness of earthquake catalogues and the hypothesis of self-similarity, *Nature, 337*, 251-253, 1989.

Sacks, S. E., and P. A. Rydelek, Quantum earthquake concept, Abstract, *Seismol. Res. Lett., 63*, 75, 1992.

Schallamach, A., How does rubber slide?, *Wear, 17*, 301-312, 1971.

Schwartz, D. P., and K. J. Coppersmith, Fault behavior and characteristic earthquakes: Examples from the Wasatch and San Andreas fault zones, *J. Geophys. Res., 89*, 5681-5698, 1984.

Segall, P., and Y. Du, How similar were the 1934 and 1966 Parkfield earthquakes?, *J. Geophys. Res., 98*, 4527-4538, 1993.

Shaw, E. B., Complexity in a spatially uniform continuum fault model, *Geophy. Res. Lett., 21*, 1983-1986, 1994.

Sibson, R. H., Implications of fault-valve behavior for rupture nucleation and recurrence, *Tectonophysics, 211*, 283-293, 1992.

Sibson, R. H., J. McMoore and A. H. Rankine, Seismic pumping--A hydrothermal fluid transport mechanism, *J. Geol. Soc. London, 131*, 653-659, 1975.

Singh, S. K., M. Rodriguez, and L. Esteva, Statistics of small earthquakes and frequency of occurrence of large earthquakes along the Mexican subduction zone, *Bull. Seismol. Soc. Am., 73*, 1779-1796, 1983.

Sleep, N. H., Ductile creep, compaction and rate and state dependent friction within major fault zone, *J. Geophys. Res.*, this issue.

Sleep, N. H., and M. L. Blanpied, Creep, compaction and the weak rheology of major faults, *Nature, 359*, 687-692, 1992.

Stuart, W. D., Forecast model for large and great earthquakes in Southern California, *J. Geophys. Res., 91*, 13,771-13,786, 1986.

Stuart, W. D., and G. M. Mavko, Earthquake instability on a strike-slip fault, *J. Geophys. Res., 84*, 2153-2160, 1979.

Stuart, W. D., R. J. Archuleta, and A. G. Lindh, Forecast model for moderate earthquakes near Parkfield, California, *J. Geophys. Res., 90*, 592-604, 1985.

Trifu, C.-I., and M. Radulian, Frequency-magnitude distribution of earthquakes in Vrancea: Relevance for a discrete model, *J. Geophys. Res., 96*, 4301-4311, 1991.

Tse, S. T., and J. R. Rice, Crustal earthquake instability in relation to the depth variation of frictional slip properties, *J. Geophys. Res., 91*, 9452-9472, 1986.

Virieux, J., and R. Madariaga, Dynamic faulting studied by a finite difference method, *Bull. Seismol. Soc. Am., 72*, 345-369, 1982.

Wesnousky, S. G., Seismological and structural evolution of strike-slip faults, *Nature, 335*, 340-343, 1988.

Wesnousky, S. G., The Gutenberg-Richter or characteristic earthquake distribution, which is it?, *Bull. Seismol. Soc. Am., 84*, 1940-1959, 1994.

Yamashita, T., Application of fracture mechanics to the simulation of seismicity and recurrence of characteristic earthquakes on a fault, *J. Geophys. Res., 98*, 12,019-12,032, 1993.

Yamashita, T., and L. Knopoff, Model for intermediate-term precursory clustering of earthquakes, *J. Geophys. Res., 97*, 19,873-19,879, 1992.

Y. Ben-Zion and J. R. Rice, Department of Earth and Planetary Sciences, Harvard University, Cambridge, MA 02138. (e-mail: benzion@geophysics.harvard.edu)

(Received February 11, 1994; revised november 16, 1994; accepted November 17, 1994.)